Scanning Microscopy

Volume 1993
Number 7 *Physics of Generation and Detection of Signals Used for Microcharacterization*

Article 7

1993

Environmental Scanning Electron Microscope: Some Critical Issues

G. D. Danilatos
ESEM Research Laboratory, Australia

Scanning Microscopy Supplement 7, 1993 (Pages 57-80) 0892-953X/93$5.00+.25
Scanning Microscopy International, Chicago (AMF O'Hare), IL 60666 USA

ENVIRONMENTAL SCANNING ELECTRON MICROSCOPE: SOME CRITICAL ISSUES

G. D. Danilatos

ESEM Research Laboratory, 98 Brighton Boulevard
North Bondi (Sydney), NSW 2026, Australia
Phone No.: (+61 2) 302837, Fax No.: (+61 2) 3650326

Abstract

In the environmental scanning electron microscope (ESEM), the gas flow around the main pressure limiting aperture establishes a density gradient through which the electron beam passes. Electron beam losses occur in this transition region and in the uniform gas layer above the specimen surface. In the oligo-scattering regime, the electron distribution consists of a widely scattered fraction of electrons surrounding an intact focussed probe. Secondary electrons are multiplied by means of gaseous ionization and detected both by the ionization current and the accompanying gaseous scintillation. The distribution of secondary electrons is governed by the applied external electric and magnetic fields and by electron diffusion in the gas. Backscattered electrons are detected both by means of the gaseous detection device and by solid scintillating detectors. Uncoated solid detectors offer the lowest signal-to-noise ratio especially under low beam accelerating voltages. The lowest pressure of operation with uncoated detectors has been expanded by the deliberate introduction of a gaseous discharge near the detector. Gaseous scintillation also offers the possibility of low noise detection and signal discrimination. The "absorbed specimen current" mode is re-examined in the conditions of ESEM. It is found that the current flowing through the specimen is not the contrast forming mechanism: it is all the electric carriers in motion that induce signals on the surrounding electrodes. The electric conductivity of the specimen may affect the contrast only indirectly, i.e., as a secondary, not a primary process. The ESEM can operate under any environment including high and low pressure, low or rough vacuum and high vacuum; it operates at both high and low beam accelerating voltage so that it may be considered as the universal instrument for virtually any application previously accessible or not to the conventional SEM.

Key Words: Environmental scanning electron microscope (ESEM), low vacuum, low-voltage SEM, electron detectors, electron diffusion, secondary electrons, backscattered electrons, gaseous detection device, scintillating detectors, detector efficiency, noise, resolution, contrast, charging.

Introduction

The environmental scanning electron microscope (ESEM) is applied to diverse fields of science and has been described in numerous reports. The possibility of examining specimens under the electron beam inside a gaseous environment has introduced novel ideas and a better understanding of the electron beam physics. The evolution of this field has been slow; early attempts date back to the beginnings of electron microscopy. The longest part of the history of this development involved the transmission electron microscope, and, during the last two decades, work has concentrated around the scanning electron microscope (SEM). The literature of these developments can be traced through a number of extended surveys (Moretz, 1973; Parsons *et al.*, 1974; Danilatos, 1982, 1988, 1991a).

The practice of operation of ESEM has turned out to involve some relatively simple methods, but the underlying physical phenomena have proved, on many occasions, difficult to understand as they involve some complex physical processes. Therefore, it is not surprising that some erroneous ideas appear from time to time. Some misunderstandings of the conventional SEM have contributed to these difficulties, and there is a continual need to update our ideas as new work and results appear from the use and theory of ESEM. However, a few authors still seem to overlook or not properly understand certain issues that were thought to have been adequately dealt with previously. In this context, the present survey aims at examining a selection of topics that are important in our understanding for the further development of the field.

Gas dynamics science is mandatory to apply to these studies. The flow of gas around the vicinity of the final pressure limiting aperture (PLA1), in particular, can affect the performance of the instrument.

The way contrast and resolution is affected by the introduction of gas must be clarified. This is done by examining the electron beam scattering and distribution in the gas and how this affects the spot size and current. The role of detectors in contrast and resolution is surveyed.

New detection methods, such as gaseous detection

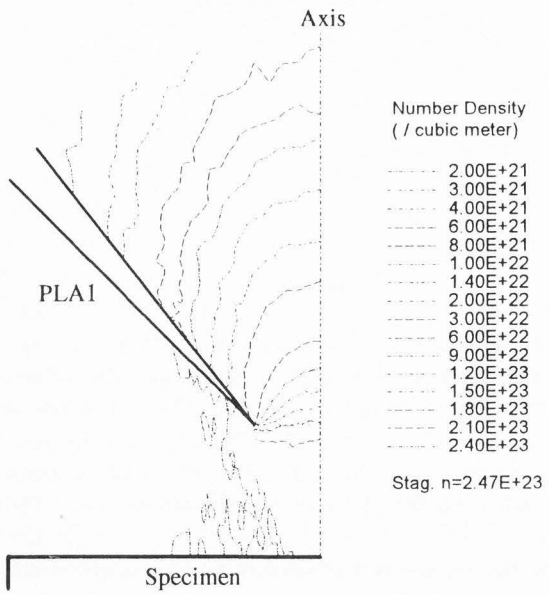

Figure 1. Number density contours of argon flowing through conical pressure limiting aperture (PLA1) with a sharp tip and with a flat specimen placed one diameter below the aperture. Stagnation number density value corresponds to 1000 Pa, and diameter of aperture is 0.4 mm. The contour values decrease monotonically in the direction of the flow.

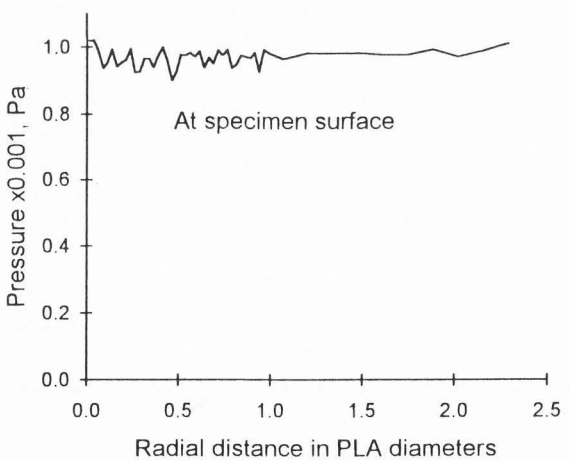

Figure 2. Variation of pressure at the surface of specimen in Figure 1 along radial distance from the system-axis.

---

and the notion of "specimen absorbed current" are re-examined. The use of uncoated scintillating materials is shown to be a good choice for low-keV work, as they demonstrate the best signal-to-noise ratio (SNR). Some new results are integrated with the discussion of these topics, and an attempt to summarize our present understanding is made.

The bulk of this paper deals with each of these topics in sufficient detail. New results and ideas are included in the course of this examination. It is only towards the end of the paper, in the **Discussion** section, that some of the issues are connected with work of previous authors in a critical way.

Mass Thickness of the Gaseous Environment

A high-pressure environment can be maintained in the specimen chamber of ESEM by use of differential pumping through a series of apertures. The electron beam can freely travel along the electron optical-axis but, as it approaches the final pressure limiting aperture (PLA1), losses of electrons due to scattering with the gas can start becoming significant. Hence, there has been a need to determine the flow field of gas especially around the vicinity of the PLA1, i.e., both below and above it (Danilatos, 1991b).

The direct simulation Monte Carlo (DSMC) method developed by Bird (1978) for gaseous flows has been used in this study. This method allows the determination of the flow field around various shapes of PLA1. One particular case is shown in Figure 1 with a conically shaped aperture and a flat specimen placed one diameter below the aperture (D = 400 μm). The iso-density contours of the field are drawn only on half of the plane containing the aperture-axis, because the flow is axially symmetric. A depletion zone is formed below the aperture, and the gas jet formed above it has a significant density up to a certain point. The effects of flow on the specimen surface can be seen by plotting the pressure at the specimen level along a direction normal to the axis as is shown in Figure 2. At the specimen distance, the pressure has decreased only by about 4% from the stagnation specimen chamber pressure of p_0 = 1000 Pa (measured with a pressure gauge at the chamber wall). This decrease takes place directly under the area of the aperture; the ragged variation of the curve is due to statistical fluctuation and is smoothed out as we increase the computation time or the number of statistical samples. The variation of density (in particles per unit volume) along the axis of the aperture is shown in Figure 3. For this plot, the number density n has been normalized over the stagnation value n_0 corresponding to pressure p_0. From this type of information, we can calculate the mass thickness of gas through which the electron beam has to pass. The definite integral:

$$\zeta = \int_z^h \frac{n(z)}{n_0} \frac{dz}{D} \qquad (1)$$

gives the normalized number thickness ζ of a gas layer along the axis from a point z up to a maximum distance h above the aperture, for which data is available and at which the pressure has decreased to a sufficiently low value. Above this point, scattering should not be significant for a properly designed instrument, but the number thickness can be calculated from the uniform background pressure p_1 prevailing at this pumping stage and the distance H between the two pressure limiting apertures. Similarly, the number thickness can be found from the constant pressure relationship for any gas layer below one diameter from the aperture. The important thing is to establish the parameter for various lengths $l = h - z$ in the transition region of pressure. For the example produced here, we plot the numerical evaluation of the integral versus z/D in Figure 4, taken in the transition region from $z = -1D$ up to a fixed value of $z = h = 3D$. We note that $\zeta = 0.48$ for $l = h$, i.e., for the mass of gas above the plane of the aperture with 40° inside cone angle; this is a little above the value of 0.4 found in the case of a flat aperture. The conical shape of the aperture is chosen for various reasons: it allows better specimen movement and ventilation, better positioning of scintillating detectors and better efficiency in the detection of pure secondary electrons (SE) with the gaseous detection device. At the specimen surface ($z = -1D$), the number thickness is $\zeta = 1.4$, and, therefore, the thickness above the aperture alone represents about 34% of the total amount. The significance of these numbers in absolute terms will become apparent as we examine the electron beam scattering below. The values of ζ are applicable to all mechanically similar flow fields, e.g., we can vary p_0 and D but keep their product p_0D constant. For practical purposes, a small deviation from the constancy of this product can be allowed, e.g., we can keep the aperture constant and vary the pressure from a few mbar to about 20 mbar. As we depart from this range, we can see the effects of the transition from free molecule flow to continuum flow. Also, for the purposes of this paper only, we consider the same number density characteristic to be applicable for nitrogen, used in some examples below. More detailed information on different gas flow fields will be reported in a specialized paper.

Electron Beam Scattering

The electron beam scattering process in the gas is governed by the Poisson distribution probability function, which gives the probability for an electron to undergo x number of collisions:

$$P(x) = \frac{m^x e^{-m}}{x!}. \qquad (2)$$

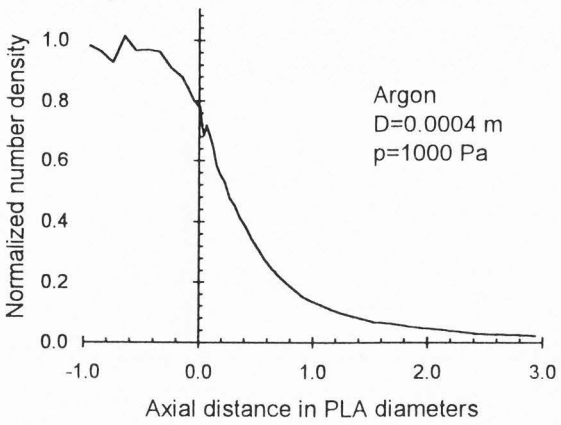

Figure 3. Variation of gas density along the axis of pressure limiting aperture for argon at 1000 Pa specimen chamber pressure.

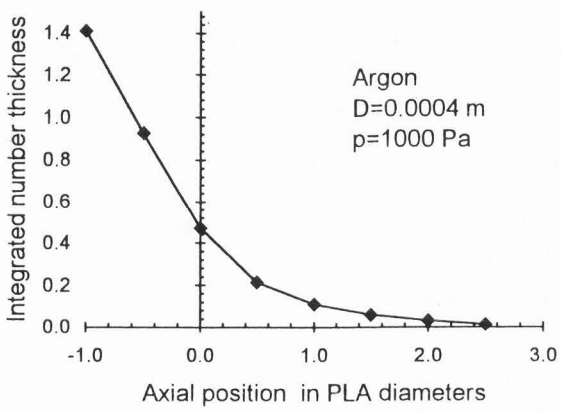

Figure 4. Integrated number thickness from a given point on the axis up to three diameters above the pressure limiting aperture.

This means that for each electron there is a probability with which it may undergo no scattering event, or a single scattering, a double scattering, etc. If the average number of scattering events per electron is m, then there is a fraction of electron beam I/I_0 that is transmitted without any scattering at all, the intensity of which decreases exponentially with m:

$$\frac{I}{I_0} = e^{-m} \equiv q. \qquad (3)$$

The parameter m is generally given by

$$m = \sigma_T \int n(z)dz, \qquad (4)$$

where σ_T is the total scattering cross-section for a given gas. For the total travel distance between specimen and

PLA2 (i.e., the PLA above PLA1) we distinguish three terms below, namely, the first m_0 for the uniform gas layer between the specimen and the beginning of the transition region, the second term m_t for the entire transition region and the third term m_1 for the uniform layer from the end of the transition region to PLA2:

$$\begin{aligned} m &= m_0 + m_t + m_1 \\ \therefore\ m &= \sigma_T n_0 (L-D) \\ &\quad + \sigma_T \int_{-D}^{h} n(z)dz + \sigma_T n_1 (H-h), \end{aligned} \tag{5}$$

where L is the distance of the specimen from the PLA1, H the distance between PLA1 and PLA2 and n_1 the background uniform (or average) number density between the two apertures. For the middle term of the transition region we get

$$m_t = \sigma_T n_0 D\zeta = \sigma_T \frac{p_0 D}{kT}\,\zeta, \tag{6}$$

where k is Boltzman's constant and T the absolute temperature. From this, we find that scattering is directly proportional to the diameter of PLAl for a fixed specimen chamber pressure. Thus, if we want to maintain the specimen as close as possible to the PLA1 with minimum gas flow influence (i.e., at one diameter), then equation (6) is the main governing relationship for the beam scattering.

The next most significant factor to consider is the electron scattering cross-section, which strongly depends on the accelerating voltage for a given gas. We still do not have precise values for this parameter for the commonly used gases in the range of accelerating voltages applicable to ESEM. One attempt to calculate it for several molecular gases was made by Danilatos (1988), and some of these values are chosen below to help us illustrate the present work. Scattering cross-sections are still due to be determined experimentally once and for all. There are indications that the theoretical values may be an overestimate of the real situation, but the present analysis will still be applicable for when we finally obtain the correct values. For now, let us consider nitrogen for three cases of beam keV as illustrated in Table 1.

We see that even with a low beam voltage of E = 5 keV, we still get 25% totally unaffected beam through the nitrogen gas at the typical pressure of 1000 Pa (= 10 mbar). Depending on the initial beam current, it has been shown that the unscattered fraction of beam can be used in the normal way for imaging. The main remaining question is whether the scattered fraction of electrons interferes with the imaging process. This question has been thoroughly examined by Danilatos (1988). It has

Table 1. Electron beam transmission in nitrogen.

		I/I_0		
E keV	σ_Tx10^{21} m^2	p=100 Pa	p=1000 Pa	p=2000 Pa
5	10.1	0.87	0.25	0.06
10	5.7	0.92	0.45	0.20
20	3.1	0.96	0.65	0.42

been shown that the scattered fraction forms a broad "skirt", orders of magnitude larger than the useful spot. It is because of this separation of the two distributions, namely, that of the focussed spot and that of the surrounding skirt, that ESEM has become possible. In scanning transmission electron microscopy, we find an effective beam spot spread, simply because the scattered fraction closely overlaps with the un-scattered fraction during the very short travel distance in the thin-and-dense specimen sections. This results in the well known "top-bottom" effect (sharper image at the top than at the bottom), but this must be set aside from the different scattering regime of our case. In ESEM, the beam travels through a layer of gas which is orders of magnitude thicker and orders of magnitude less dense than the solid specimens of transmission microscopy. This has prompted us to define the "oligo-scattering" regime in ESEM which incorporates the single scattering and the early part of the plural-scattering regime. Plural scattering includes between 1 and 25 scattering events and multiple scattering more than 25 scattering events (Cosslett and Thomas, 1964). Strictly speaking, a single-scattering regime should be defined as that where most electrons (say 95%) undergo either one (single) or no collision at all. From equation (2), we find that this corresponds to $m < 0.35$, whereas for $m = 1$, we find that 37% of electrons undergo no collisions, 37% undergo a single collision, 18% two collisions, 6% three collisions, etc. Clearly, it is possible to practice ESEM for m up to 2 or, perhaps, a little more; $m = 3$ corresponds to 95% of the original beam removed and has been defined (arbitrarily) as the upper limit of the oligo-scattering regime. Concomitant with this definition we should add that the travel distance in the gas should be set such as to make the separation of the skirt from the useful spot feasible.

If the resolving power of the instrument is identified (or related) with the beam spot diameter, then we can state that this is not affected by the presence of gas. With a resolution test specimen producing sufficient contrast, we have repeatedly confirmed this (Danilatos, 1990b, 1991a). In fact, the smaller the original spot, the better separation we obtain. Lanthanum hexaboride electron gun sources are better than tungsten, and field emission guns are even better in this regard. However,

resolution for a general specimen is intimately connected with the available contrast. The presence of the broad electron skirt affects the contrast of the image by way of adding a "white" background noise level, and this negative effect is exacerbated by the weakening of beam intensity. The contrast can be recovered by simply increasing the beam current by an appropriate amount, and the quantitative relationships for this to occur have been presented previously (Danilatos, 1988). An increase of beam current is, of course, accompanied by a larger beam spot, and, to this degree, the resolution will deteriorate. However, with a large class of applications such high resolutions are not needed or we may be prevented from reaching a very high magnification by other overriding considerations such as beam specimen damage. Finally, contrast and resolution at this level are intimately connected with the detection systems used, as will be outlined below.

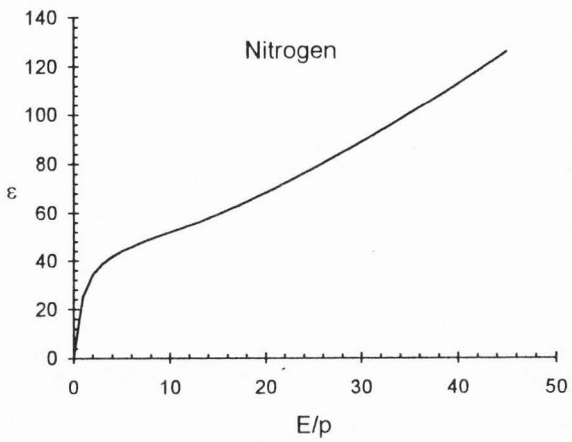

Figure 5. Variation of parameter ε versus E/p.

Secondary Electron Diffusion

The presence of gas in the ESEM has necessitated the design of novel detection systems as well as the appropriate adaptation of conventional ones. The conventional secondary electron detector is not suitable for operation in the gaseous environment of ESEM. However, the secondary electron signal can still be retrieved, amplified and used. There have been many works on this novel development, and reference to them will help in the better understanding of the present survey (Danilatos, 1983, 1990a, 1990b, 1990c).

The motion of secondary electrons inside a gas is governed primarily by diffusion and by the electric and magnetic fields applied or formed around. It is well known that these electrons have an energy around 2 eV, and only a small fraction of them have sufficient energy to ionize and excite gas molecules directly. Depending on the nature of the gas, there is also a small probability for an electron to attach itself to a gas molecule to form a negative ion. These possibilities and others have been surveyed in detail previously (Danilatos, 1990a). In the main, the electrons remain free to diffuse among the surrounding gas molecules. If an electric field is present, then they will also move in the direction of the field at the same time.

By considering the electron/gas collision process, it can be easily shown that the SE (with energies around 2 eV) lose only a very small fraction of their energy with each elastic collision (mass of electron being much smaller than mass of gas molecule). The electrons behave like a gas, and, in the absence of an external electric field, they would come in equilibrium with the host gas. However, even in the presence of a weak field, they immediately acquire a few eV energy. This energy of electrons expressed as kinetic energy, $mv^2/2$, is far beyond the kinetic energy of the gas, which is of the order of $3kT/2$. Because of the weak exchange of energy between the electron gas and the host gas, the electrons have their own diffusion pattern, which is different from the pattern of other bulky ions that may form around. In the calculation of electron diffusion, the ratio of the electron energy over the gas energy enters as a parameter ε:

$$\varepsilon = \frac{mv^2}{2} / \frac{3kT}{2}. \qquad (7)$$

The variation of ε versus E/p (E being the intensity of the electric field) has been measured by several workers for various gases and their results have been compiled by Danilatos (1990a). One particular example is considered in Figure 5 for nitrogen. The combined effect of thermal diffusion and field attraction can easily be seen in the case of a uniform field between two parallel electrodes as shown in Figure 6.

At the bottom electrode, there is a point source of electrons S like the SE generated at the specimen surface. For this simple case, the distribution of electrons, as they arrive at the top electrode, has been derived by Huxley and Zaazou (1949). When the potential difference is increased beyond a certain level for a particular gas, the electrons acquire sufficient energy to excite and ionize the gas molecules. The electrons then multiply by an avalanche process, but it can be shown that the distribution of all the electrons together remains the same as in the case of low field. The fraction of electrons R arriving within a radius r at the top electrode is given by

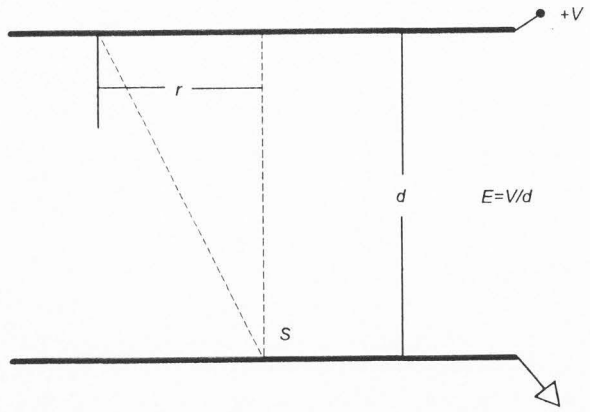

Figure 6. Uniform electric field E between two plane electrodes having a potential difference V and a point electron source at S.

$$R = 1 - \left[1 + \frac{r^2}{d^2}\right]^{-1/2} \cdot \exp\left\{\frac{eV}{2kT\varepsilon}\left[1 - \left[1 + \frac{r^2}{d^2}\right]^{1/2}\right]\right\}. \quad (8)$$

We note that R is a function of the ratio r/d versus which we can plot the result at fixed values of the parameter ratio V/ε. To better illustrate the situation, we can choose different fixed bias V in Volts for the typical case where $pd = 1$ Pa · m (e.g., at $p = 1000$ Pa and $d = 1$ mm). The results are shown in Figure 7. Unfortunately, we still do not have data on ε for high values of bias, and the dotted line has been calculated from an arbitrary extrapolation for ε according to $\varepsilon = 36 + 1.73(E/p)$. For very low bias, below 1 Volt, all curves coincide with the one for $V = 1$ Volt, because the variation of ε can be approximated by a straight line passing through the origin of the axes in Figure 5. For low values of bias, the diffusion plays a major part in the distribution of electrons. As we increase the bias, their distribution becomes significantly narrower. According to Wilkinson (1950), the electrons tend to follow the lines of force for high values of E/p.

The distribution of ions generated at high fields is simply that of SE because the ions do not diffuse much further: they are practically as bulky as the neutral molecules and quickly come to thermal equilibrium after each collision, i.e., they lose their energy acquired from the external field between successive collisions (there is a strong coupling and $\varepsilon \approx 1$). The ions do not create additional ionization, as their energy is converted to thermal movement.

The equations of electron and ion distribution in the

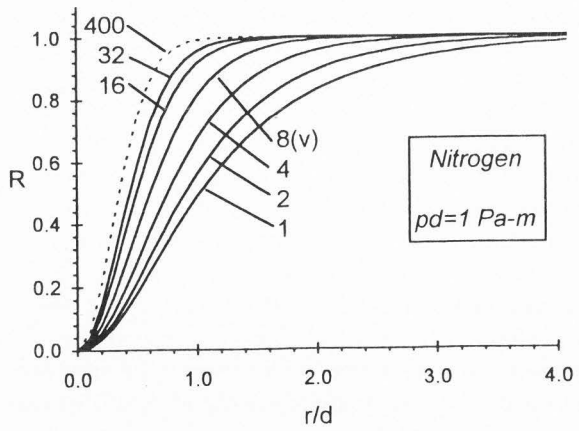

Figure 7. Variation of R versus r/d for different fixed values of electrode bias V at constant $pd = 1$ Pa · m.

ESEM and the corresponding induced signals have been derived previously. The backscattered electrons have their own corresponding distribution of charge and their own induced signal. It has been shown that the two signals can be separated by use of appropriate electrode configurations (Danilatos, 1990a, 1990b, 1990c).

Noise Propagation in Detection Systems

The theory, practice and literature of SNR for various detection systems in SEM have been surveyed elsewhere (Jones, 1959; Wells, 1974; Reimer, 1985). Following the same principles, we can outline the situation for two basic detection systems used in ESEM, namely, the gaseous detection device and solid scintillating detectors.

Gaseous detection device

The gaseous detection device (GDD) is based on the detection of products of interaction between various signals and gas. Initially, the ionization of gas was used to produce images, and later, it was demonstrated that the gaseous scintillation could also be used for the same purpose. We consider both of these approaches.

Ionization. For a given beam current I_0 and pixel dwell time r, we get n_0 electrons striking the specimen at each pixel element when the specimen chamber is in vacuum. For a given SNR K and M gray levels on the recorded micrograph, we find the following relationship (Wells, 1974):

$$I_0 = \frac{K^2M^2e}{4\tau}\left[\frac{\sqrt{\delta_A + \delta_B} + \sqrt{\delta_B}}{\delta_A}\right]^2, \quad (9)$$

where e is the electron charge, δ_A is the fraction of the electron beam that is converted to useful signal (or feature) after the beam-specimen interaction and δ_B is the fraction that is converted to background noise. When we introduce gas, the above equation is modified as follows (Danilatos, 1988):

$$I_0 = \frac{K^2 M^2 e}{4\tau} \left[\frac{\sqrt{\delta_A+\delta_B+\delta_0} + \sqrt{(1-q)\delta_A+\delta_B+\delta_0}}{q\delta_A} \right]^2 , \quad (10)$$

where δ_0 represents the ionization electrons in the gas generated by the beam before the beam strikes the specimen; this constitutes one of three terms adding to the background noise level. The second term is simply $q\delta_B$ from the useful spot. The third term is generated from the skirt fraction $1 - q$ of electrons striking the specimen (the primary electrons back-scattered from the gas are neglected because they constitute an extremely small fraction under the oligo-scattering condition). For the skirt electrons striking the specimen, the conversion coefficient δ_S depends on the precise specimen nature, the magnification used and the extent of the skirt. A conservative value of $\delta_S = \delta_A + \delta_B$ has been taken for the derivation of equation (10), but this can be adjusted accordingly; for a general purpose analysis of the detection system, the above assumption can be satisfactory. For a graphical presentation below, the last two terms relate to the specimen nature and, lumped together, are designated as $\delta_{BB} \equiv q\delta_B + (1 - q)\delta_S = (1 - q)\delta_A + \delta_B$.

We can now depict the signal propagation in the detection system as in Figure 8. Let us consider a case with a 20 keV beam, PLA-specimen distance d = 0.0004 m, and nitrogen gas with 2000 Pa pressure. In vacuum, the incident beam delivers $n_0 = I_0\tau/e$ particles at each pixel element, which can be normalized to unity (stage No. 0). In the presence of gas, we get to stage No. 1 just before the beam strikes the specimen; for this, we plot first the number in the useful spot q = 0.42, on which we add the skirt $1 - q$, on which we finally add the primary beam effect δ_0. We find that $\delta_0 = S_0 pd$, where S_0, the ionization efficiency of the beam, depends on the accelerating voltage; for the present case, we take S_0 = 0.13 ions/Pa · m and find $\delta_0 \approx 0.1$. In the following stage No. 2 (beam-specimen interaction), we first plot the useful signal $q\delta_A$, on which we add δ_{BB} for the point above, on which we finally add δ_0 to obtain the top point. We have taken, as an example, $\delta_A = \delta_B$ = 0.1. Following this, we consider the gaseous amplification to arrive at stage No. 3. The gaseous gain can be calculated for each component of electrons at stage 2. We can readily get an amplification factor $e^{\alpha d} - 1$ for all the SE originating at the specimen surface and an amplification factor $(e^{\alpha d} - 1)/\alpha d$ for δ_0 (Danilatos, 1990b),

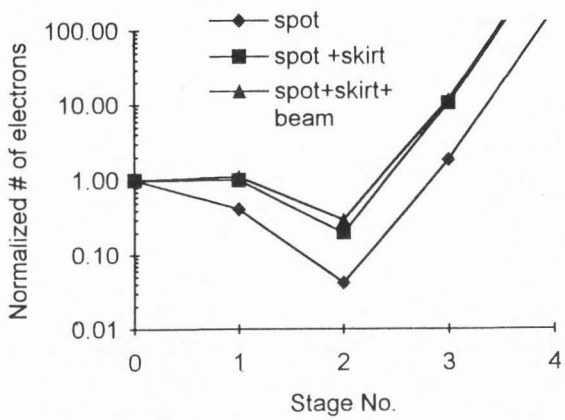

Figure 8. Gaseous detection device (ionization). Relative variation of number of electrons at various stages for the useful "spot", the "skirt" (interacting with specimen) and "beam" (interacting with gas before it strikes the specimen). The noise bottleneck is at the beam-specimen interaction.

---

where α, the first Townsend coefficient, is given by

$$\alpha = Ap \exp\left[-\frac{B}{V} pd \right] \quad (11)$$

with A and B constants tabulated for each gas. For nitrogen, with electrode bias V = 400 Volts, we get for the first Townsend coefficient α = 9479 ions/m. Thus, the gain factor for δ_0 is 11.9, whereas the "spot + skirt" signal has a gain factor 43.7. Therefore, the beam effect tends to be suppressed relative to all SE electrons originating from the specimen surface, which receive a preferential amplification.

From the scheme in Figure 8 we see that the noise bottleneck is at the beam-specimen interaction. The main consideration after this is the noise introduced by the operational amplifier at stage 4. If the equivalent-input noise of this amplifier is greater than the noise at stage 3, then the system is limited by the amplifier. Therefore, every effort should be made to choose an amplifier with the best possible characteristics and also to try to obtain the maximum possible gaseous gain with the GDD. The gaseous amplification is associated with very low noise and is to be preferred over the subsequent operational amplifier's gain. Future development should concentrate on extracting a higher gain from the GDD.

To simplify the above analysis, the ionization caused by the backscattered electrons (BSE) has not been mentioned. The BSE from the specimen also create a primary ionization in the bulk of the gas, which is

amplified by the external field. However, the latter can be separated out by proper electrode configuration, and the remaining component adds only a small fraction of additional signal which has been omitted from the present scheme (see details in Danilatos, 1990a, 1990b, 1990c).

Scintillation. It has been shown that we can use the gaseous scintillation from the signal-gas interactions to form images (Danilatos, 1986). When we apply a strong electric field, the cascade electrons in the gas, apart from ionization, also liberate photons which multiply in an analogous way. This has been used to produce secondary electron images by simply collecting the gaseous scintillation with a suitable light-pipe/ photomultiplier (PMT) system (Danilatos, 1992). The gaseous scintillation thus produced is usually much stronger than the specimen cathodoluminescence (CL) which does not present a problem. However, in some cases, a strong CL may be superimposed, especially when a simple PMT is used. In future work, spectroscopic methods and other means can be used to separate out the various sources of signal. The use of known CL methods in the gaseous environment of ESEM can lead to alternative microanalytical techniques.

For the present, the use of a PMT is a best replacement for the operational amplifier used with the ionization GDD, because a PMT adds practically no background noise (typical anode dark current is a few nA at a gain of 10^6). The signal propagation in the scintillation GDD is shown in Figure 9. Here, we plot the total signal, namely, that of "spot + skirt + beam". For illustration purposes, we may assume that for each cascade electron we also get one photon (the actual situation varies with the applied bias and the nature of gas). Thus, the stages up to No. 3 have been drawn identical with those of Figure 8. Stage 4 is the collection of photons from the gas by an appropriate system. We may assume that we can collect at least one quarter of the total. Of these, 40% may be transmitted through the light pipe (stage 5) and 15% are converted to photoelectrons at stage 6 (Wells, 1974). The PMT can then produce a gain of up to 10^6 at stage 7. The dotted line shows the case where we manage to collect twice as many photons in the gas and improve the photoelectron conversion also by a factor of two. It is evident that a second noise bottleneck can appear, and every effort should be made to improve the photon collection and transmission efficiency of this detector. After this, the main play is with the gaseous gain on which this system mainly relies. Once we shift the second "dip" clearly above the level of stage 2, we obtain one of the simplest and most powerful detection systems for ESEM.

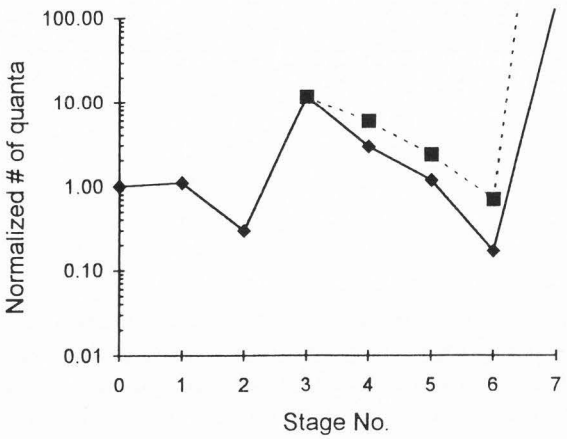

Figure 9. Scintillation gaseous detection device. Propagation of the total signal through various stages. Two noise bottlenecks may compete with each other. Dotted line is one improvement starting with same gaseous gain as with the ionization GDD.

Solid scintillating BSE detectors

The signal propagation through various stages for a solid scintillating detection BSE system is depicted in Figure 10. The situation is qualitatively the same up to stage 2 as in the previous case. The total signal, here, is that of "spot + skirt". The electrons from the initial beam-gas interaction (δ_0 factor) are omitted, because they are of very low energy and do not excite the (unbiased) detector. In this figure, we analyze and compare a typical SEM case with an improved situation aimed at in ESEM. Usually, not all of the BSE from stage 2 are collected by the detector, and it is not uncommon to collect about half of the total. The loss is represented with a lower value at the "collection" stage 3. It is also customary in SEM to coat the detector with an aluminum coating. This layer can absorb a significant amount of signal energy, especially when we wish to operate the microscope at low accelerating voltage, say below 5 keV. This situation can easily account for a loss of more than half of the total BSE signal energy. The aluminum coating has a beneficial effect by eliminating the low-energy BSE; when we use higher accelerating voltages, in the high-magnification range, then the high-energy fraction of BSE is practically transmitted through, minus a small percentage of it that is itself backscattered from the coating out of the detector. The latter reason alone is sufficient to make us plot the number of transmitted BSE with a slightly decreased value at the next stage, No. 4 (e.g., 10% less). The main loss of signal as a result of the coating will appear in the next stage (stage 5) in the form of a smaller number of

photon quanta than would otherwise be produced. Stage 5 (scintillation) represents a net gain by the conversion of the remaining electron energy to photons. If 2% of the electron energy is convened to photons and if each photon takes 3.1 eV (Wells, 1974), then we expect an amplification of about 10 in this process, for an electron energy around 1.5 keV (presumed to pass through the aluminum coating by use of a 5 keV incident beam). Following this, we expect to have some serious losses again: in the light pipe, we may be left with about 40% of the initial light (stage 6), which is considered a good transmission rate. About 15% of the photon quanta produce photoelectrons at the PMT photocathode (stage 7). From this point, we expect a huge gain by the PMT of the order of 10^6 (stage 8).

In ESEM, it is possible to have a much improved situation, simply because we can dispose of the aluminum or other conductive coatings on the detector and because we can improve the BSE collection angle to its maximum possible. The mass thickness of a 70 nm aluminum coating is 189 $\mu g/m^2$, whereas that of a nitrogen layer 1 mm thick at 100 Pa is only 1.15 $\mu g/m^2$. This gas layer, or even much less, is sufficient to neutralize the accumulated negative charge on the detector, as will be shown in the next section. This allows us to use a significantly lower keV beam. Because charging is not a problem, we can bring the tip of the detector close to the edge of the PLA1. The dotted line in Figure 10 shows stage 3 with 90% of the signal collected. Stage 4 is omitted. Improved scintillation efficiency (about double) can be gained by use of YAG/YAP crystals (Autrata *et al.*, 1983), and such an increase is incorporated in stage 5. There is also scope to optimize the shape of the detector to increase the light transmission to the maximum possible (Danilatos, 1985); in this example, we use a 40% transmission rate again. Last, the coupling between detector and PMT can also be improved to increase the signal conversion, and a factor twice as high has been used in this plot. This and other measures to improve the efficiency of the detector will be reported in more detail separately.

The analysis of signal propagation clearly indicates that there is good scope in making every effort to improve the collection and propagation of signal in the detector itself. This allows us to operate the ESEM at low beam keV.

Charge Neutralization, Low-Vacuum SEM, Low-Voltage SEM and Universal ESEM

Occasionally, concern is expressed about the capability of the ESEM to operate at low-vacuum or at usual-vacuum SEM condition. It is thought that the GDD ceases to operate at low vacuum, and an uncoated

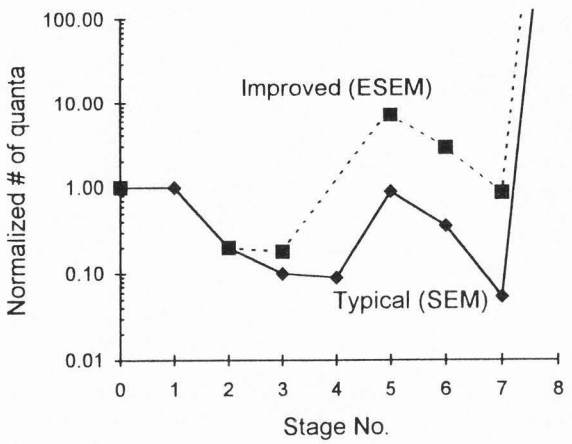

Figure 10. Solid scintillating detectors in conventional SEM and a possible improvement in ESEM. Signal propagation at various stages. Two bottlenecks can appear at low-keV operation.

---

scintillating detector would charge up. Until recently, every effort was consumed with making the ESEM capable of operating under as high a pressure environment as possible. However, it can be shown both in practice and in principle that the ESEM can also operate under vacuum or low-vacuum condition.

The operation of GDD does not depend on the gas pressure alone but rather on the product of (pressure) x (distance) or *pd*. Therefore, when the pressure decreases, we can increase the specimen/electrode distance in inverse proportion to maintain the maximum detector signal. Depending on the design of GDD, the distance of specimen/electrode may be separate from the distance of specimen/PLA1. Of course, other effects, such as electron diffusion, should be taken into account and properly counteracted in various designs. If the GDD electrode is small, an increasing fraction of electrons can be lost as we increase the specimen distance, according to equation (8). Also, a sharp-tip PLA, used as an electrode, produces a non-uniform electric field and can result in losses by diffusion. This problem can be remedied with the use of a multi-electrode GDD (Danilatos, 1990a, 1990b, 1990c). A second concentric electrode around the tip of the PLA can be used for the separation and detection of BSE electrons at sufficiently short specimen distances from PLA1. When the distance is increased, this second electrode becomes a SE detector also. A special configuration of a multi-electrode scheme is shown in Figure 11; the first electrode is the PLA1, and the second is made from a metal grid or grids attached (or deposited) onto a scintillating detector. The same arrangement is repeated around the PLA2. This electrode configuration caters for any specimen

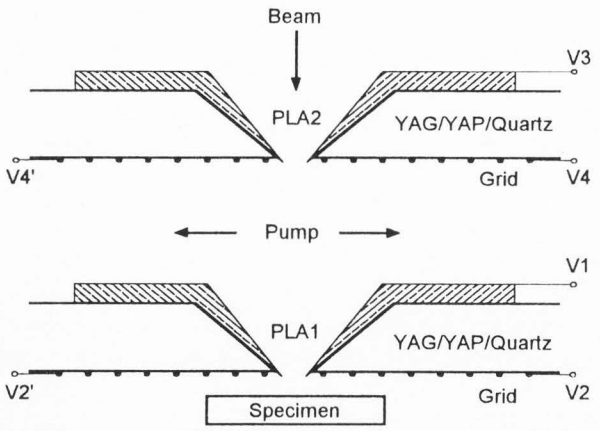

Figure 11. Universal ESEM. Integrated GDD with solid scintillators and PLAs to operate from vacuum to high-pressure environment, at low and high beam voltage, with a variety of detection modes.

---

distance. Differing types and fractions of signals between BSE and SE are detected as we vary the specimen distance from a relatively long to a relatively short distance from the PLA1. Each electrode is biased independently with Vl, V2, V3 and V4 Volts. At the cost of some electronics complexity, we can gain valuable flexibility by splitting each grid in two separate electrodes biased with V2' and V4' Volts.

The gaseous gain of GDD has been analyzed and found to exhibit a maximum for some value of pd, which is usually around 1 Pa · m. This maximum depends on the precise gas composition and electrode configuration. Depending on the gas used, for a specimen distance of 10 mm, the pressure can be lowered down to around 50 Pa without changing the electrode bias. Theoretically, we can further increase the distance and decrease the pressure, but this is generally undesirable because the electron beam aberrations also increase. Alternatively, we can fix the specimen distance and increase the bias to achieve sufficient gain. This may not be at the characteristic maximum of gain curve observed as we vary the *pd*. Eventually, this parameter (bias) is also exhausted as the number of ionizing collisions becomes practically very low or zero. At this point, we can turn to other imaging modes, namely, to scintillating detectors and to biasing the attached electrodes in the keV range so as to accelerate the slow electrons as in the conventional SEM. A very high bias on the grids will also act as an electrostatic lens for the incident beam, and, hence, we may require additional screening grids not shown in Figure 11.

As we decrease the pressure, we need to inquire at which point do we lose all the benefits of ESEM and fully convert to conventional SEM conditions. The first benefit that is given up is the wet specimen condition (below 609 Pa). However, there is still great interest in observing other gaseous reactions at lower pressures or simply using the gas as a charge suppression agent. Let us, therefore, inquire about the limits of charge neutralization in ESEM. With a conductive specimen, the final limiting factor would be the presence of the uncoated scintillating detectors, the benefits of which were outlined in the previous section. Scintillating detectors integrated with the GDD and PLAs are shown in Figure 11. The shapes are those calculated by Danilatos (1985) and at least one pair of such detectors are integrated with PLA1 and another pair with PLA2. Ideally, four detectors at each plane would greatly increase signal collection and manipulation and system flexibility. The electrode grids are sufficiently thin to allow the maximum possible free area of detector exposed to the incidence of BSE. At very short working distances, a large fraction of BSE escapes through the PLA1 and is detected by the system of detectors at PLA2.

The negative charging artifacts in vacuum SEM usually arise from the excess negative charge retained by insulating objects. In ESEM, this charge accumulation is effectively suppressed by the ionized gas and, in particular, by the positive ions in the gas. We may distinguish between the negative charges created by all the fast electrons that "stick" on the insulating surfaces and the "mobile" slow electrons that can easily be repelled and diffuse away. The fast electrons (beam and BSE) forcefully accumulate on the neighboring surfaces which would resist any further contribution from the slow electrons. The slow electrons are further assisted to disperse away by their high mobility in the hot "electron gas". Conversely, the positive ions are much less mobile; they constitute a gas in near equilibrium with the host gas and are attracted by the negatively charged areas. Hence, if there is a sufficient number of ions around, they will effectively "neutralize" those areas. With some exceptional specimens, the ions generally would just balance the negative charge, because any additional accumulation of positive charges would tend to repel new ones from approaching. In the end, we can have effective charge suppression and any positive or negative charges in excess for this suppression move away to finally dissipate on the nearest conductive surface. The exception to this general process occurs when we deal with very extended insulating specimens within a very restricted region and in the presence of confining electric and magnetic fields; then, positive charge

accumulation occurs on the specimen. Here, we shall deal with only the usual and general case where negative charging occurs by the "sticking" fast electrons.

The general movement just described above takes place in the absence of any biased GDD electrodes. When we introduce such electrodes, as in Figure 11, they act as "sinks" for various charges. If we bias the electrodes positively, the mobile slow electrons need not travel far, as they are directed towards these electrodes by the field. The ions would still travel towards the negatively charging areas to neutralize them, and any excess will diffuse away to the nearest ground surface. What we need now is to find the relationship of various parameters for the generation of ionization current in the gas. This current (I_i) is caused by the incident beam, the BSE and SE as in the three terms of the following equation (Danilatos, 1990b):

$$I_i = I_0 \left[\frac{pS_0}{\alpha} + \frac{2\eta\, pS_{BSE}}{\alpha} + \delta \right] (e^{\alpha d} - 1), \qquad (12)$$

where η is the BSE coefficient, δ the SE coefficient and S_{BSE} the ionization efficiency of the BSE. We can normalize the ionization current by dividing by the beam current and, considering equation (11), we obtain

$$\frac{I_i}{I_0} = \left[\frac{S_0 + 2\eta S_{BSE}}{A \exp\left[-\frac{B}{V} pd \right]} + \delta \right] \left\{ \exp\left[Apd \exp\left[-\frac{B}{V} pd \right] \right] - 1 \right\}. \qquad (13)$$

The above equation incorporates the additional ionization caused by the external field through bias V, in the absence of which we have only the primary ionization from the beam and BSE. The latter case can be directly derived, or reduced from equation (13) to the simple equation

$$\frac{I_i}{I_0} = (S_0 + 2\eta S_{BSE})\, pd. \qquad (14)$$

We note that the ionization current is a function of pd against which we plot the result for two cases of accelerating beam voltage in Figures 12 and 13. For comparison purposes, we set $\delta = \eta = 0.1$, and, for nitrogen, we use $A = 9$ 1/(Pa · m) and $B = 256.5$ V/Pa · m. For the case of 5 keV beam, we use $S_0 = 0.43$ and $S_{BSE} = 0.64$, and, for 30 keV, we use $S_0 = 0.09$ and $S_{BSE} = 0.15$ (see Danilatos, 1990b). The electrode bias is fixed at 100, 200 and 300 Volts when we apply equation (13) and at 0 Volts when we apply equation (14). It should be stressed that these values are realistic, but some of these parameters may be difficult to verify by experiment. The ionization parameters are very

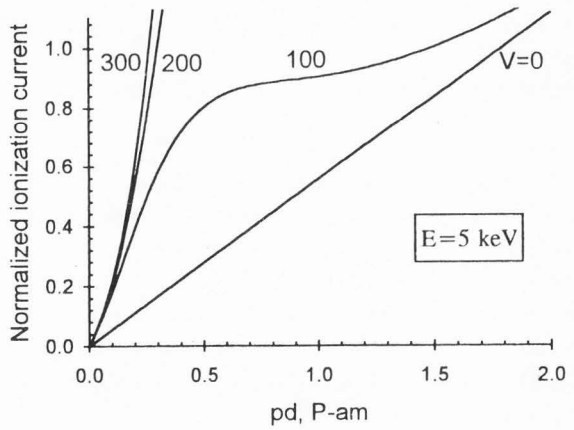

Figure 12. Variation of ionization current normalized over beam current versus *pd* at different electrode bias.

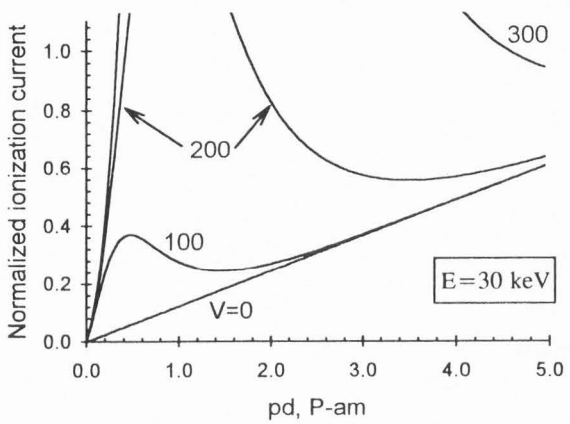

Figure 13. Variation of ionization current normalized over beam current versus *pd*, at different electrode bias.

---

sensitive to the nature of gas and gas composition which are not fixed in the ESEM. The parameters A and B have limited validity only for a specified pd range and only for pure nitrogen. Any quantitative comparison between theory and experiment also requires very accurate measurement of pressure and distance, for which we need well calibrated equipment. Also, a small component of the ionization current arises from the γ-processes, i.e., from the ions liberating additional electrons from the cathode (or specimen). When the latter component is significant, we operate near the breakdown point, and instabilities occur so that it is better not to seek gain from these processes (at least until we learn more about them); these greatly depend on the nature of the cathode, and they constitute a special topic for further research (see discussion in Danilatos, 1990a). The purpose of using and evaluating the above equations is not to obtain precise numerical

answers. The great value of these derivations is the fact that they explain the interplay of the many parameters that are involved in our system well, and, with this understanding, we discuss the results obtained. In Figure 12, we find that at $pd = 1.8$ Pa · m enough ion current is produced to neutralize the total beam current in the absence of any bias ($V = 0$ Volts). In fact, we need less ion current if we assume that the SE diffuse away and even less ion current to neutralize the negative charge of the BSE on the detector alone. First, let us consider no bias on the electrode ($V = 0$): For $\eta = 0.1$ we find that we need only $pd = 0.2$ Pa · m (see Figure 12), which is consistent with results on image distortion due to charging published previously (Danilatos, 1988). For the 30 keV case (Figure 13), we find that $pd = 8.1$ Pa · m is needed to neutralize the total beam current and only $pd = 0.8$ Pa · m for the detector alone.

The most important finding from the graphs in Figures 12 and 13 is that charge neutralization is achieved much easier when we apply bias to the GDD electrode. From Figure 12, we find that only $pd = 0.06$ Pa · m is needed to neutralize the detector when we apply 100 V to the electrode; only marginal improvement is found with higher bias. The situation is similar in Figure 13 where we get $pd = 0.09$ Pa · m with 100 V and a slightly less value for higher bias. The precise values will vary with actual specimen nature, gas composition and electrode geometry. The important finding here is that we can benefit greatly by simply accompanying our uncoated BSE detectors with a biased electrode in order to generate and supply additional ions, over and above those produced by the primary ionization of the beam and BSE alone.

Initially, one simple approach to achieve the above benefit is to employ the BSE detectors together with the PLA1 (or PLA2) electrode alone. When we bias this electrode positively, most of the mobile slow electrons will be dissipated on it. Thus, we will be left mainly with the BSE and beam electrons that "stick" on the nearby surfaces which can be neutralized by the generated ions. When the electrode grids on the detectors are also present, they may be grounded or slightly biased negatively to attract positive ions in their direction. It may be preferable to bias the PLA1 electrode with the minimum positive voltage required only to suppress charging and thus keep gaseous scintillation to a minimum. Usually, the solid detector is producing much more intense light, and the gas is not expected to interfere. Alternatively, the gaseous scintillation can be controlled by the gas composition used. With the use of various electrodes and biases, the shaping of the electric field can vary to achieve a desired result. There are many parameters that we can control, which is an advantage, as each application's needs can be catered for accordingly. It is beyond the purposes of this paper to exhaust all the possibilities now open.

The main conclusions and observations above have been confirmed by experiment. For example, sharp-tip electrodes have been successfully used, and they can coexist next to and in contact with plastic materials. Detection above the PLA1 has also been reported (Danilatos, 1985, 1990d). In this case, the PLA1 electrode can act as a control "grid" to manipulate the fractions of signal passing through the aperture and also as a "sink" for the positive ions forming above the aperture. In the ElectroScan ESEM, where differential pumping is incorporated within the objective lens, we expect to achieve additional gaseous gain as the charges tend to move in helical paths (due to magnetic field), and their effective path is lengthened in the low pressure region above the PLA1.

Until recently, we have placed emphasis on making the ESEM operate at as high of a pressure as possible. Currently, we have extended our research work to cover the region of low-vacuum and vacuum regime in order to cater for specialized applications that still need those conditions. The behaviour of an uncoated BSE detector with a suitable grid electrode has not yet been fully tested in conventional SEM vacuum. It is envisaged that, by the right choice of grid dimensions and attachment, this alone would prevent detrimental charging in vacuum. This possibility will free the ions from being used on the scintillator to being used on insulating specimens and thus extend the low-vacuum limit for such specimen applications. Alternatively, the use of a compromise thickness of aluminum or other type of conductive coating can still be considered to help us create a detection system that would cover the complete pressure range. In vacuum, we can apply bias in the keV range to accelerate the SE as in the E-T detector. This can be better achieved with the grid at PLA2 (with possibly an additional screening grid in front of it, not shown). The passage through the hole of a pole piece and the detection of the SE above the hole in SEM have been reported in numerous papers by various workers. Clearly, this possibility is also open to ESEM, and, by the appropriate specimen positioning, PLA1 size and bias, we can achieve a very good separation of the BSE from the SE signal. In conclusion, the composite detection configuration of Figure 11 can operate in vacuum, low vacuum and high pressure in the specimen chamber and thus make the ESEM a versatile, highly efficient, universal instrument.

In Figure 11, it is shown that instead of scintillating material we can use quartz to detect cathodoluminescence or gaseous scintillation. Sapphire, like quartz, also transmits in the ultra-violet region, but any other material with a desired light transmission or other

physical properties may substitute the scintillating detectors. Therefore, the possibility of using uncoated materials has freed the microscope to be fitted with alternative and new detection designs not previously possible.

Having explained the operation of ESEM in the low-vacuum regime, we can now see that it is also possible to use a low-voltage beam as well, i.e., to work towards 1 keV. Low-voltage SEM has become increasingly popular in recent publications. Low-voltage ESEM clearly offers all the advantages without any of the limitations of the SEM. A small amount of the appropriate gas present will eliminate the remaining charging artifacts of difficult specimens as those with re-entrant surfaces.

Standardization of BSE Detector Efficiencies

The new possibility of operating an uncoated and unbiased BSE detector at low-keV beam creates the need for objective measurement of the quality or efficiency of such detectors. Such a measurement should be done in a way that different detectors can be objectively compared. Those workers involved with the development of scintillating BSE detectors are usually faced with the task of evaluating the capability of a given detector and comparing it with others. It is not uncommon to see graphs of the signal "strength" for a particular detector, but this really tells us little about how this compares with work in other laboratories. Different photomultipliers even of the same kind have different characteristics and ultimately the only meaningful quantity for comparison purposes is the amount of noise that a particular detection system generates for a given signal. Each detection system has a characteristic which is determined below.

Baumann and Reimer (1981) have analyzed and measured the quality of different detectors (see also Reimer, 1985; Oatley, 1985; McLure, 1990). Following a similar procedure, we get that the relative variance $\nu(n_r)$ at stage r is a function of the variances at the previous stages as follows:

$$\nu(n_r)=\nu(n_1)+\frac{\nu(\delta_1)}{n_1}+\frac{\nu(\delta_2)}{n_1\delta_1}+\ldots+\frac{\nu(\delta_{r-1})}{n_1\delta_1\delta_2\cdots\delta_{r-2}} \quad (15)$$

where the conversion factors δ_r, for each stage relate with the number of quanta n_r between successive stages as

$$n_r = \delta_{r-1}n_{r-1}. \quad (16)$$

The test of the detector efficiency should be done at as low of a pressure as possible, and only enough gas should be used to neutralize the detector. Thus, stage 0 and stage 1 are lumped into stage No. 1. The shot noise in the beam follows a Poisson distribution, and the conversion of the beam to BSE follows a binomial distribution. These first two stages combined together follow a Poisson distribution (Reimer, 1985). Taking into account the laws of these statistics and setting $\delta_1 = \eta$, we find for the first two terms

$$\nu(n_1) + \frac{\nu(\delta_1)}{n_1} = \frac{1}{n_1\eta}. \quad (17)$$

Because the relative variance relates to the SNR as

$$\nu(n_r) = \frac{1}{K_r^2} \equiv \frac{1}{(SNR)^2_{OUT}}, \quad (18)$$

we find from equation (15) for the total system

$$\frac{1}{K_r^2} = \left[1 + \nu(\delta_2) + \ldots + \frac{\nu(\delta_{r-1})}{\delta_2\cdots\delta_{r-2}}\right]\frac{1}{n_1\eta} \quad (19)$$

One of the conversion factors, namely, at the scintillation stage (i.e., δ_3 for an uncoated and δ_4 for a coated detector) is a function of the beam voltage, so that the above expression can be written as

$$\frac{K_r^2}{n_1\eta} = \frac{K_r^2}{\eta I_0\tau/e} = \Delta(E) \quad (20)$$

where the function $\Delta(E)$ is the inverted bracketed factor of equation (19). This function can be used as the characteristic of the BSE detector. The denominator of equation (20) is simply the total number of BSE coming out of the specimen, which, on account of its Poisson statistics, can be written as

$$\frac{(SNR)_{OUT}}{(SNR)_{BSE}} = \sqrt{\Delta(E)} = \frac{K_r}{\sqrt{\eta I_0\tau/e}}. \quad (21)$$

The function $\Delta(E)$ is known as the detective quantum efficiency (DQE) with the $(SNR)_{BSE}$ taken as the SNR at the input of the detector. In the latter case, the DQE incorporates the collection stage (efficiency) of the detector, which is pertinent for our case. The theory and practice on DQE can be traced through elsewhere (Jones, 1959). For us, the practical steps to take in the evaluation of equation (21) are as follows. We need to experimentally measure $(SNR)_{OUT}$ and calculate the $(SNR)_{BSE}$ from a beam current measurement. For this, we need to use a standard (or reference) material of known η. Carbon can be chosen for the role of a reference material, for one reason because it could help in the reproducibility of measurements on account of possible contamination during measurements. A contamination layer, when present, is generally carbonaceous in nature and could alter the backscattering coefficient of

any other reference material. A thin contamination layer could then introduce a significant experimental error, especially at the very low beam voltages where we wish to detect differences in detector performance. For each value of beam voltage we measure K_{OUT}, I_0 and τ. For this, it is helpful to use as a feature the hole on a polished carbon surface over which we scan the beam at normal incidence. A smooth carbon surface can be made by depositing a carbon layer of appropriate thickness on a polished beryllium ($Z = 5$) surface (with a deep hole on it). With this, we can measure both the beam current (Faraday cage) and the output signal (corresponding to the carbon surface) from the detector with appropriate means. For this feature, we define only two gray levels ($M = 2$), one for the hole and one for the surface. It is better to use low magnification and measure the signal away from the edge of the hole so as to avoid edge effects. We should use several values of beam current of sufficiently low level to make the noise visible and measurable and find an average value of $\Delta(E)$ for the fixed E. The noise level can be measured either from a micrograph or from the electronic signal output of our detector. This measurement presents the main difficulty and, perhaps, the main reason for which DQE measurements are so scarce in the literature. If the noise is measured from a micrograph, this could be done by optical means to retrace the noise and measure the true r.m.s value of it, making sure that frequencies corresponding to spatial detail smaller than the pixel on the micrograph is rejected (i.e., variation smaller than the average resolution of the bare human eye); the time constant is that corresponding to the pixel on the micrograph. If the noise is measured by an electronic meter directly from the output of the detection system, then care should be taken to establish the time constant of the system (i.e., of the meter or the detector electronics, of both in combination). In the latter case, time constant τ is the integrating time over which the signal is being built. This time constant is the inverse of a frequency bandwidth Δf, to which some authors also refer. A relationship between these parameters is (Reimer, 1985):

$$\tau = \frac{1}{2\Delta f}. \qquad (22)$$

The same bandwidth or time constant must be used for the calculation of $(SNR)_{BSE}$ in equation (21). Perhaps, a practical way for this measurement might be to use a filter with known bandwidth and measure the r.m.s. with a meter of a much wider bandwidth.

One small complication is, however, the fact that η varies with beam voltage in the low-keV range in which we are interested. All materials seem to have this variability except for copper, which has $\eta = 0.31$ (see Reimer, 1985). We note that for the low atomic number materials there is an increase of the coefficient as we decrease the beam voltage, and we have to decide either to use the actual value of the coefficient for each beam voltage or to use an aveage value by convention. In the latter case, we could agree that the measured quantity $\Delta(E)$ is a "figure of merit", not the DQE.

The measurement of SNR is generally a difficult subject on account of other complications. For example, a "low-loss" BSE detector is not covered appropriately by the above "standard" scheme, as the parameter of specimen tilt has not been considered. Also, we have assumed that our PMTs are of good quality and operate in a bias range where its variance changes little with bias (usually above 500 Volts). Generally, we assume that all other parameters are optimum and only the beam energy varies. Even with these restrictions, our present scheme covers a broad class of scintillating BSE detectors as these are likely to be used in ESEM and SEM. The one additional parameter that must be monitored, nevertheless, is the specimen distance from the PLA1 (or from the detector, in general). The efficiency of detectors in Figure 11 shows a maximum at some optimum distance. For very short distances from the PLA1, the detectors at PLAl have decreased collection efficiency as most of the BSE escape through the hole. For a very long distance, the collection efficiency is also low because of the small subtended solid angle. Therefore, there is an optimum maximum at some point between those two positions (usually around 1 or 2 mm from PLA1).

On account of the complexity of the SNR theory and DQE measurements, the above suggestions are an attempt to discuss a practical procedure for introduction in the determination of the efficiency characteristic of various detectors.

The value of $\Delta(E)$ starts from zero and approaches unity at some high value of beam keV for a good scintillating BSE/PMT detector. It significantly departs from unity below 5 keV, and large deviations are observed around 1 keV where various detectors are expected to compete. For the E-T detector, the fixed 12-keV bias is thought to maintain the second "dip" in the SE signal propagation chain well above the noise bottleneck at the specimen (this depends on the efficiency of the particular design of detector at hand). ESEM has now ushered the possibility of using solid scintillating BSE detectors with a low-voltage beam without the need to accelerate the BSE in the keV range, as is usually done with low-voltage SEM in vacuum. In SEM, an alternative approach has been the use of the converted BSE signal to SE at the pole piece (CBSE), a detection method that has produced very good results at low-keV operation (Baumann and Reimer, 1980). It should be pointed out that a variation of the CBSE mode is also possible in ESEM and,

indeed, with certain advantages: this variation consists in using the GDD with reverse bias so that the SE from the converter plate are amplified in the gas. It remains to be seen how a well designed uncoated BSE detector in ESEM compares with alternative detection systems in the low beam voltage mode.

Discussion

Some critical aspects of the principles and operation of ESEM have been surveyed in this paper. It has been shown that significant pressure levels can be tolerated in the specimen chamber of ESEM for operation with a beam accelerating voltage of 5 keV or less. The minimum saturation water vapor pressure at 0° C is 609 Pa, a theoretical scattering cross-section at 5 keV is 7 x 10^{-21} m^2, and for a travel distance of 0.5 mm after a 0.4 mm PLA diameter, we find about 50% un-scattered transmission beam rate. In practice, the cross-section is found to be smaller, and the spot should be even better than that. Therefore, fully wet specimens at 5 keV, or lower, can be examined (Danilatos, 1988).

With regard to electron beam distribution and scattering in SEM, an attempt to investigate the situation was made by Moncrieff *et al.* (1979). From single scattering theory, they concluded that the effect of the gas was to deflect a certain proportion of electrons out of the original beam. However, this important statement was totally negated by a corresponding measurement of the beam diameter. In their same paper, Moncrieff *et al.* say: "The beam diameter was also measured from the rise-time of the transmitted signal as the beam was scanned across a sharp edge (Joy, 1974)... It was observed that a 50 nm beam, after 20 mm flight path, changes little up to a pressure of ~10 Pa. The increase in beam diameter, up to 100 nm at 133 Pa, above this pressure is indicative of the changing shape of the beam distribution. The change in slope for the onset of the beam maximum is observed experimentally as an increase in the rise-time of the transmitted signal, and this is reflected in the larger beam diameter." They also measured the scattered electron distribution with a Faraday cup and found good agreement between experiment and theory. However, this good agreement referred only to the tail of the scattered electrons, not to the immediate neighborhood of the useful spot. It could then be speculated that the single-scattering regime theory could not account for the plurally scattered electrons, which could, presumably, alter the shape of distribution at the beam diameter level. As a result, this important issue relating to the ultimate resolution of ESEM had remained unresolved until a comprehensive study was published by Danilatos (1988). In the light of that study, we can now establish the conditions under which Moncrieff *et al.* conducted their experiment for the beam diameter measurement: from the values of pressure and distance travelled, we find $m = 0.125$ at 10 Pa (with $\sigma_T = 2.54 \times 10^{-21}$ m^2 at 25 keV) and $m = 1.25$ at 100 Pa. Clearly, these values are within the oligo-scattering regime and no beam spread should have been observed. In fact, the use of a long specimen distance at 20 mm results in a wider skirt by one order of magnitude than when we use 2 mm, and the separation of useful spot from the skirt should be much more distinct. In addition, since the real cross-section for nitrogen is expected to be smaller than the theoretical value used here, the values of m for the Moncrieff *et al.* experiment should be even less (i.e., they definitely operated in the oligo-scattering regime). Their observed beam spread was probably due to contamination of the sharp edge they used, as this type of artifact was also observed by Danilatos (1988). The experimental solution to this problem was to heat the edge at a high temperature to stop a contamination finger developing.

In connection with the electron beam spread, some misunderstandings have also been published by Farley and Shah (1990a). They have suggested that, when the average number of collisions per electron equals unity (i.e., at one mean free path), we have a 100% (total) electron beam loss. This has led them to believe that the limit of imaging in ESEM occurs when $m = 1$ (presumably thinking every electron is scattered out of the beam). However, under this condition ($m = 1$), we have 63% of the electrons removed from the beam and 37% of original electrons still remaining in the original spot (see equation (3)). Our practice has shown that this can be quite adequate to operate the instrument. Therefore, their suggested limits of pressure operation are in error. They also incorrectly claim that their results agree with Danilatos (1988). However, their paper closely repeats the work by Moncrieff *et al.* (1979).

Farley and Shah (1990a) claim that the inelastically scattered electrons influence the beam current density profile, and hence, they deteriorate resolution. They generally believe that "in high-pressure SEM...the beam profile and electron current distribution on the specimen surface are altered" and that this affects the resolution of the image.

Shah and Beckett (1979) used an environmental cell for the study of wet botanical specimens. Notwithstanding the value of that publication along with those of other workers that preceded it, we are compelled to make a reappraisal of the early ideas put forward, especially in view of their continual repetition (until recently) by the same group. In their first paper, they used a differentially pumped environmental cell in conjunction with the "absorbed specimen current" mode for imaging. That system was named "moist environment ambient

temperature scanning electron microscope" or MEATSEM. Moisture was perceived as a necessary and sufficient condition of MEATSEM in order to maintain the specimen conductivity and, hence, make the specimen current mode feasible. This condition was clearly spelt throughout the paper as, for example, they say: "The stage essentially incorporates differentially pumped chambers which allow the specimen to remain conducting, during the operation of the microscope, for a comparatively long period, keeping it at ambient saturated vapour pressure of water"; and further, "MEATSEM avoids this type of damage because the higher electrical conductivity of the moisture content of the specimens eliminates the need for metal coating". However, in our present understanding, this is not necessary (Danilatos, 1983, 1990a, 1990b, 1990c). The presence of gaseous ionization was totally overlooked, or its role mistaken by Shah's group for many years later: Shah (1987) says, for example,: "...Forming an image under these conditions presents formidable difficulties. The conventional technique of constructing an image by secondary electrons does not work because secondary electrons, primary electrons and back-scattered electrons ionize water or gas molecules close to the specimen and produce additional electrons. These electrons, which do not carry any information about the specimen surface, have a similar energy range to that of the secondary electrons emitted from the specimen, so they cannot be separated easily from the secondary electrons released from the specimen surface. Without such separation, there is a severe deterioration of the secondary emitted image...". Clearly, such views are not helpful and caution is required when referring to these works. The use of ionization to suppress charging artifacts was previously known and used by several authors (Pfefferkorn *et al.*, 1972; Parsons *et al.*, 1974; Moncrieff *et al.*, 1978). The use of ionization for imaging purposes was first introduced by Danilatos (1983). This was first applied to the commercial ElectroScan ESEM for secondary electron imaging in early 1986.

Shah has recently acknowledged the use of ionization as an imaging means, but this is still confused with the notion of the conventional specimen current mode for imaging. In recent articles, another acronym, HPSEM ("high pressure SEM"), was introduced to essentially refer to MEATSEM (Shah *et al.*, 1990; Farley and Shah, 1990a, 1990b). Those authors still advocate that "specimen current imaging ...can be usefully applied to high-pressure SEM since it does not rely on the interception of the emissive electrons or the physical amplification of the signal within the specimen chamber" (Farley and Shah, 1990b). In other words, the emissive modes are thought to be intercepted by the gas, whereas the specimen current is not. This clearly explains their concept of specimen current, which, flowing through the specimen, is not affected by the gas (their idea). This, of course, does not explain the last remark in that same paper that, under charge neutralization, "no net specimen current flows into or out of the surface," and it does not explain how their imaging is possible with their specimen current mode when no specimen current is present. Such ideas seriously overlook the true natural processes occurring in the microscope, and they are clearly set apart from our own understanding. We advocate that contrast is formed by induction during the flight of all charges between electrodes, i.e., by displacement current (Danilatos, 1990a, 1990b, 1990c). The flow of current through the specimen should be taken into account when we balance the total charge. Accumulation of charge can still be present in certain cases, and the conductivity of the specimen can influence the final contrast, but the "specimen absorbed current mode" does not really exist in its own right as an imaging mode per se. Charging and specimen current, to the extent they occur, are after-effects in the final image formation.

In Figure 7, we have considered the effect of diffusion on the total current collected by two plane electrodes. Other effects, such as recombination and space charge, have been discussed in detail and found not to contribute to any significant degree in the conditions of ESEM. However, Farley and Shah (1990a, 1990b) believe that these factors control the signal intensity or quality. For space charge, in particular, they write: "In the absence of any electric field the ionic carriers form an accumulation of space charge above the specimen which can inhibit or distort the emission of the secondary electrons or the collection of low-energy ionic carriers. To counter the action of the space charges, it is necessary to extract them from the vicinity of the specimen. This can be done by an electric extraction field provided by a biased electrode placed above the specimen". The "space charge" notion is heavily promoted throughout that paper (Farley and Shah, 1990b) which otherwise merely repeats the work by Moncrieff *et al.* (1978). According to the literature surveyed and our own experience, the present author has reported that space charge is of no concern in the ESEM, especially at low electrode bias (Danilatos, 1990a). Space charge effects can appear within individual avalanches at the head of the avalanche, at very high electrode bias only under specialized conditions of very high gaseous gain. However, the positive ions can pose a problem **only because of a possible accumulation on the specimen surface**, especially with very large and extended flat insulating specimens below a flat anode electrode. For this problem, we have employed an additional electrode

above the specimen surface as an ion controller, or sink, for any excess positive ions. A fraction of positive ions is attracted by the specimen surface tending to become negative by the electron beam bombardment (negative charge neutralization), and the rest of the positive ions find their way to the nearest conducting surface (acting as a cathode). If such a surface is very far away, we should provide one closer to prevent positive charge accumulation on the specimen surface, and this will result in an improvement of contrast. **The improved contrast is caused by the higher gaseous gain attainable, as the effective field is maintained high when the positive ions cannot accumulate on the insulating surface.** When they accumulate on the surface, the effective field is reduced, and the signal gain deteriorates. The true nature of phenomena ought to be clearly understood, if we are to improve the performance of the GDD.

The signal propagation characteristic of the ionization GDD in Figure 8 shows the real and potential advantages of this method. For a low gaseous gain, the noise bottleneck shown can be superseded by the equivalent-input noise current of the operational amplifier. With a GDD gain factor up to 100, beam currents well below 100 pA are commonly used in ESEM. Several orders of magnitude higher gaseous gain has been achieved with equivalent nuclear devices, and hence, we can expect significant improvements in future designs of GDD (see extensive review of nuclear devices by Danilatos, 1990a). At present, the main limitation arises from our desire to use water vapor in many applications, but for another class of applications, for which water vapor is not required, high gains should be achievable. Generally, any improvement in the gaseous gain, even by small amounts, is very significant and desirable for this device.

The scintillation GDD holds great promise because of the very low noise level of the associated PMT. If every care is taken to optimize the scintillation of the gas as well as the optical coupling and light transmission from the light source to the PMT, then we can expect some excellent SNR characteristics.

The early work on ESEM involved the use of plastic scintillating detectors, and this prompted a conscious development of these detectors. The aim was to increase the detective quantum efficiency of the detectors in order to compensate for the loss of signal from the beam-gas scattering. Also, those detectors had to be reshaped and redesigned generally to make them fit in the restricted region of operation of the prototype machine. It became apparent that the shape of these detectors could easily become critical and could result in serious light loss, which, in turn, would create a second noise bottleneck. That was indeed the case with early shapes of BSE detectors. Optimum shapes that would fit in a particular prototype were reported later (Danilatos, 1985). In Figure 10, it is clearly shown how critical the detector design becomes for low-keV operation, a quality that is highly sought in ESEM, especially for beam sensitive materials. The first factor that can be improved is the BSE collection angle. Here, we refer to that fraction of BSE associated with a particular type of information and with a particular spatial or atomic number resolution; no consideration is given on how the various fractions of electrons are separated, something that has been the subject of study by the electron microscopy community for a very long time. Most recent reports have quoted resolutions below 1 nm by use of a wide angle BSE (Autrata, 1990, 1992). The concept of using a wide angle BSE detector has been supported by various workers, but we must separate this concept from Robinson's ideas and practice (Robinson, 1973, 1974). Robinson advocates that "the complete rediffused electron signal must be detected, using a 2π geometric rediffused electron detector" and "...that collection of the total rediffused electron signal gives the same resolution as the secondary electron signal...". In practice, Robinson has used a large (near hemispherical) piece of bulk scintillating detector with a large hole in it for the passage of the beam. This subtends a wide angle at the specimen. However, the images with this design show directionality of illumination (shadowing), which is indicative of loss of BSE signal from the side of the detector across the light pipe. Some workers mask a portion of the more efficient side of this detector to make the image uniform, but all this shows is that the employed shape with a single PMT is significantly less than optimum. The high resolutions recently observed with the use of more efficient BSE detectors are now generally attributed to the "Murata peak" (Murata, 1974). The reason for resurfacing this old topic is because there is a need to improve the efficiency of BSE detection in ESEM and to show that there is scope for further improvements of BSE designs. For example, the hemispherical type of bulk scintillating detector with a hole in it and a single PMT is inefficient (or insufficient) in ESEM. The hole in the detector cannot become less than the PLA1. In ESEM, the specimen may be placed close to the PLA1, and most of BSEs are concentrated in a small region of the order of the PLA diameter. Small variations (i.e., fraction of mm) in the detector machining or positioning can result in large deviations from optimum signal in ESEM. The light pipe design and the presence of the hole present serious obstacles, and the end result is that we can have large BSE signal loss followed by large light loss in the light pipe. The situation is greatly improved by a calculated shape of the detector and by use of two detectors instead of one. Much better results by way of efficiency and signal

manipulation could be achieved by a system of four detectors. The high-resolution "Murata peak" is associated with a low BSE function of the total signal, and only an efficient detector would render this signal visible. A low efficiency detector uses additional BSE electrons from and towards the tail of the spatial electron distribution and the resolution deteriorates.

The need for efficient solid scintillating detectors in ESEM has prompted us to propose a standard way for objectively measuring the efficiency of these detectors. The same method, namely, the measurement of $\Delta(E)$, could be used for all BSE detectors in general except that this can also be dependent on the beam current used. The case that we analyzed in this paper is applicable to detectors with good PMT which have very low anode dark current. If we use operating amplifiers instead, then the efficiency characteristic will also depend on the beam current, generally speaking, and, hence, we should consider $\Delta(E,I)$ as the appropriate characteristic. For our present needs, we need to incorporate the specimen distance as an additional parameter: $\Delta(E,L)$.

One main aspect of the present survey is the advance of the universal detection system in Figure 11. An important ingredient of this detection configuration is the introduction of an "ion generator" by means of a biased electrode in the neighborhood of uncoated scintillating detectors. This extends the operation of ESEM down to relatively very low pressures, much lower than without a controlled discharge. A self-controlling discharge usually results in an erratic or irregular charge suppression which becomes evident on the image as an instability as we decrease pressure. For example, the value of $pd = 0.06$ Pa · m implies that for a specimen distance of 10 mm we can operate down to a 0.06 mbar pressure. By carefully choosing the gas mixture, this pressure could be even lower. Therefore, we can bridge the gap between the vacuum of the conventional SEM and the usual high-pressure environment of the ESEM. This is a novel approach that has come as a "spin-off" from the development of the GDD. Moncrieff *et al.* (1978) experimented with the measurement of the ionization current of the gaseous discharge only for the purpose of determining the effective negative bias that automatically forms on insulating specimens from the electron beam bombardment. They concluded that a discharge was automatically forming as the specimen was charging to about -140 V by the incident electron beam, and the residual gas in the specimen chamber was sufficient for the purpose. Until the present time, one member of that group still uses and still considers both the aluminum coating and a metal liner in the large hole of the detector as necessary elements for wide angle plastic scintillating detectors (Robinson, 1980). The deliberate introduction of a controlled gaseous discharge at low and intermediate vacuum, as suggested here, can significantly improve the performance of detectors.

The main conclusion on the BSE detectors is that ESEM has created the unique opportunity of detecting the BSE signal with uncoated and unbiased solid detectors at beam accelerating voltages well below 5 keV. Already, the low-voltage SEM (in vacuum) has demonstrated its value but also its limitations with regard to the type of specimens and range of beam keV. The possibility of charge suppression at intermediate vacuum also implies the possibility of using low beam voltage in ESEM without the hurdles and limitations of vacuum SEM. In the near future, practice will show the merits of this new approach in electron microscopy.

We need to clarify that we should not resist using some of the conventional methods of SEM, if some applications require us to do so; all these methods can be incorporated in the ESEM. For example, if we wish to image hot specimens with YAG/YAP detectors, then we have to coat the detectors with aluminum to prevent the hot stage light from interfering with imaging. The ionization GDD is, of course, capable of operating in the presence of light. Also, we can easily incorporate the conventional E-T detector, should its presence be required. If some applications have to have long working distances, or very high tilt or other manipulation that is used in SEM, then ESEM can also incorporate these parameters, with the understanding that some of the advantages that the ESEM offers per se may have to be compromised or sacrificed. Any of the specimen preparation techniques, or a modification of these, can be applied to ESEM also. In conclusion, the ESEM is in no way lacking when compared to the conventional SEM. The latter is a subset of the former.

All imaging has been omitted from the present report, as this needs to be systematic with each separate topic. A detailed examination of all these topics, simultaneously, would fall outside our original aim. The different topics surveyed in this report have only been outlined and discussed in order to facilitate better understanding and to invite further contributions from other workers. There are still many questions open, and many aspects require further analysis and experimental support. New results are planned to be reported in due course.

Conclusions

The electron beam in the ESEM splits in two fractions as it travels through the gas layer to reach the specimen. One fraction remains focussed in the same spot that forms in vacuum and the other function forms a broad scattered electron skirt around the focussed spot.

This defines the oligo-scattering regime of ESEM. The focussed spot can be used for imaging in the usual way while the skirt adds a background noise level. The resolving power is limited by the probe size which remains constant as we increase the chamber pressure. Only when we are forced to increase the contrast by increasing the beam current do we sacrifice resolution on account of beam diameter increase. However, for a large number of applications in ESEM we rarely need beam diameter magnifications.

The gaseous detection device has replaced the conventional SE detector. At present, the GDD is used in two modes, namely, the ionization and the scintillation mode. Both these modes can produce SE and BSE imaging. In addition, solid scintillating detectors have been developed to produce high-SNR imaging. The high efficiency is achieved by specially calculated shapes and by their ability to operate uncoated. This ability is greatly enhanced by deliberately providing a gaseous discharge in the neighborhood of the active surface of the detectors. The signal propagation of all these detection systems has shown that they produce some of the best SNR features. Their efficiency coupled with their ability to image the natural surfaces of virtually any specimen produces new types of contrast and new information in practically every field of application of this microscope. The ESEM has become the universal instrument for operation virtually under any environment including vacuum, low vacuum and high pressure as well as low-and high-voltage microscopy.

References

Autrata R (1990) New configurations of single-crystal scintillator detectors in SEM. In: Electron Microscopy 1990, Proc. XIIth Int. Congr. El. Microsc. Vol. I. Peachey LD, Williams DB (eds.). San Francisco Press, 376-377.

Autrata R (1992) Single crystal detector suitable for high resolution scanning electron microscopy. EMSA Bulletin, Vol. **22**(2), 54-58.

Autrata R, Schauer P, Kvapil Jos, Kvapil J (1983) Single-crystal aluminates - a new generation of scintillators for scanning electron microscopes and transparent screens in electron optical devices. Scanning Electron Microsc. **1983**;II, 489-500.

Baumann W, Reimer L (1981) Comparison of the noise of different electron detection systems using a scintillator-photomultiplier combination. Scanning **4**, 141-151.

Bird GA (1978) Monte Carlo simulation of gas flows. Ann. Rev. Fluid Mech. **10**, 11-31.

Cosslett VE and Thomas RN (1964) The plural scattering of 20 keV electrons. Brit. J. Appl. Phys. **15**, 235-248.

Danilatos GD (1982) The environmental scanning electron microscope and its applications. Scanning Electron Microsc. **1982**;1, 1-16.

Danilatos GD (1983) A gaseous detector device for an environmental SEM. Micron and Microscopica Acta **14**, 307-318.

Danilatos GD (1985) Design and construction of an atmospheric or environmental SEM (Part 3). Scanning **7**, 26-42.

Danilatos GD (1986) Cathodoluminescence and gaseous scintillation in the environmental SEM. Scanning **8**, 279-284.

Danilatos GD (1988) Foundations of environmental scanning electron microscopy. Adv. Electronics Electron Phys. **71**, 109-250.

Danilatos GD (1990a) Theory of the gaseous detector device in the environmental scanning electron microscope. Adv. Electronics Electron Phys. **78**, 1-102.

Danilatos GD (1990b) Equations of charge distribution in the environmental scanning electron microscope (ESEM). Scanning Microscopy **4**, 799-823.

Danilatos GD (1990c) Mechanisms of detection and imaging in the ESEM. J. Microsc. **160**, 9-19.

Danilatos GD (1990d) Design and construction of an environmental scanning electron microscope (Part 4). Scanning **12**, 23-27.

Danilatos GD (1991a) Review and outline of environmental SEM at present. J. Microsc. **162**, 391-402.

Danilatos GD (1991b) Gas flow properties in the environmental SEM. Microbeam Analysis--1991. Howitt DG (ed.). San Francisco Press, 201-203.

Danilatos GD (1992) Secondary electron imaging by scintillating gaseous detection device. Proc. 50th Annual EMSA Meeting. Bailey GW, Bentley J, Small A (eds.). San Francisco Press, 1302-1303.

Farley AN, Shah JS (1990a) Primary considerations for image enhancement in high-pressure scanning electron microscopy (1. Electron beam scattering and contrast). J. Microsc. **158**, 379-388.

Farley AN, Shah JS (1990b) Primary considerations for image enhancement in high-pressure scanning electron microscopy (2. Image contrast). J. Microsc. **158**, 389-401.

Huxley LHG, Zaazou AA (1949) Experimental and theoretical studies of slow electrons in air. Proc. Roy. Soc. Lond. **196**, 402-426.

Jones RC (1959) Quantum efficiency of detectors for visible and infrared radiation. Adv. Electronics and Electron Phys. **11**, 87-183.

Joy DA (1974) SEM parameters and their measurements. Scanning Electron Microsc. **1**, 327-334.

McLure SG (1990) Backscattered electron imaging.

M.Sc. Thesis, La Trobe University.

Moncrieff DA, Robinson VNE, Barker PR (1978) Charge neutralization of insulating surfaces in the SEM by gas ionization. J. Phys. D: Appl. Phys. **11**, 2315-2325.

Moncrieff DA, Barker PR, Robinson VNE (1979) Electron scattering by gas in the scanning electron microscope. J. Phys. D: Appl. Phys. **12**, 481-488.

Moretz RC (1973) Electron microscopy of biological materials in the natural state. Ph.D. Thesis, State University of New York at Buffalo.

Murata K (1974) Spatial distribution of backscattered electron in the scanning electron microscope and electron microprobe. J. Appl. Phys. **45**, 4110-4117.

Oatley CW (1985) The detective quantum efficiency of the scintillator/photomultiplier in the scanning electron microscope. J. Microsc. **139**, 153-166.

Parsons DF, Matricardi VR, Moretz RC, Turner JN (1974) Electron microscopy and diffraction of wet unstained and unfixed biological objects. Adv. Biol. Med. Phys. **15**, 161-271.

Pfefferkorn GE, Gruter H, Pfautsch M (1972) Observations on the prevention of specimen charging. Scanning Electron Microsc. **1972**, 147-152.

Reimer L (1985) Scanning Electron Microscopy. Springer-Verlag, Berlin, 137.

Robinson VNE (1973) A reappraisal of the complete electron emission spectrum in scanning electron microscopy. J. Phys. D: Appl. Phys. **6**, L105-L107.

Robinson VNE (1974) The construction and uses of an efficient backscattered electron detector for scanning electron microscopy. J. Phys. E:Sci. Instr. **7**, 650-652.

Robinson VNE (1980) Electron microscope backscattered electron detectors, U.S. Patent 4217495. Aug. 12, 1980.

Shah J (1987) Electron microscopy comes to life, No. 208/1987/SPECTRUM, 6-9. Central Office of Information, London, UK (available by British Embassy or Consulate).

Shah JS, Beckett A (1979) A preliminary evaluation of moist environment ambient temperature scanning electron microscopy. Micron **10**, 13-23.

Shah JS, Durkin R, Farley AN (1990) Scattering of electrons at high-pressure and restoration of image contrast in high pressure scanning electron microscopy. In: Electron Microscopy 1990, Proc. XIIth Int. Congr. El. Microsc. Vol I. Peachey LD, Williams DB (eds.). San Francisco Press, 384-385.

Wells OC (1974) Scanning Electron Microscopy. McGraw-Hill Book Company, New York, pp 20-36.

Wilkinson DH (1950) Ionization Chambers and Counters. Cambridge University Press, Cambridge, 38.

Discussion with Reviewers

M. Kotera: In gaseous detection, a potential is applied between the specimen and the detector. A kind of plasma is excited in the field. The electric field is not linear in the region, and the field may be large close to the specimen surface. Then, positive ions, which are ionized by electron bombardment, hit the specimen surface with relatively large energy. Is there higher possibility for the specimen to get damaged by the bombardment?

Author: The kind of plasma situation that you refer to does not occur in our system. We only have a weakly ionized gas with the present gaseous gain of the GDD and with the low electron beam currents used. In future work, we will attempt to obtain a few orders of magnitude higher gain and then your question could become more relevant. At present, sometimes we have the opposite effect: with extended flat insulating surfaces, in a uniform electric field, we have a net positive charge accumulation **on the specimen surface**, which results in a decreased total electric field, which corresponds to a lower gaseous gain and lower amount of ions. With respect to the mechanisms of specimen damage for when it occurs, we have done little study up to the present [see Danilatos GD (1986) Beam-radiation effects on wool in the ESEM. Proc. 44th Annual Meeting EMSA, 674-675]. The ion-specimen interaction will be followed with great interest in the future.

M. Kotera: It seems that images obtained by the gaseous detector and those obtained by the solid state detector show differently because of the difference in the imaging mechanisms. Is it possible to estimate or evaluate what kind of information can be revealed by the difference? and why is that?

Author: Unfortunately, I have not seen any comparison between images obtained by solid state detectors and GDD published . I cannot comment on this yet. Tentatively, I may suggest that the solid state detector images are BSE images, whereas those that you might have seen from GDD are SE images.

A. Dubus: You conclude your paper by writing: "The ESEM has become the universal instrument for operation...". How do you look to the future of this particular technique?

Author: As I have stated on numerous occasions, the ESEM is the natural extension of SEM; the former is destined to replace the latter in its traditional applications, and, in addition, it has opened many new areas of application not previously accessible to SEM. With reference to other microscopical techniques, ESEM is again

destined to play its role, because it can give types of information not accessible to those techniques either. The fact that magnification ranges may overlap between various techniques is irrelevant, because each technique has its own merits, advantages and disadvantages. I do not see various microscopical techniques as "competing" with each other. I see all those techniques rather as complementing each other.

J.M. Cowley: What is the relationship of the detector system to the objective lens pole-pieces? If the detector electrode distances are increased, as proposed, will this not decrease the resolution by increasing the focal length of the lens?

Author: With reference to Figure 11, the lower set of BSE detectors can be placed just below (abutting with the bottom face of the lower pole-piece of the objective lens), as is currently done. The upper set of detectors can be integrated inside the objective lens. This suggested configuration is a general one, and the specific dimensions can be varied to allow integration with the lens. The ESEM requirements are outlined herewith, first, so as they can be incorporated in future generations of instruments.

The resolution will decrease by increasing the focal length of the lens. My comment of increased specimen distance is referred to those workers demanding such increased working distances, in order to accommodate large specimen tilting or for other reasons. The preferred working distance in ESEM is a short one, in order to allow high gas pressure and, fortuitously, better resolutions. In fact, the GDD is ideally suited for such short working distances, and hence, ESEM is promising to produce the best possible resolution with a given electron optics column.

R. Autrata: In the section "Solid scintillating BSE detectors", you report that 2% of the electron energy is transformed into photons in the scintillating material. According to Figure 11, this material is YAG or YAP. The conversion radiation efficiency ξ = 2% was reported by O.C. Wells (1974, p. 33) for the plastic scintillator, type Pilot. It is, however, known that for YAG it amounts to 4-5% (Takeda *et al.* (1980) J. Electrochem. Soc. **127**, 438) and for YAP ξ = 6-7% (Autrata *et al.* (1984) Proc. 8th European Congr. on EM. Vol. 1. p. 167). Precise values of radiation efficiency depend on the technology of preparation of scintillators. Can a higher value of ξ influence your evaluations of efficiency of your detection systems. And how?

Author: In Figure 11, I am proposing the use of YAG/YAP crystals, but the calculations for a typical SEM in Figure 10 were done for a plastic scintillator, as per reference given. For the ESEM graph in Figure 10, I have used ξ = 4% as an example for possible improvement. You are stating that we can have an even better improvement than this, which is, of course, most welcome. I have tried to demonstrate in this paper that a high conversion efficiency material is highly sought for low-voltage work, and the use of good grade YAP materials are planned to be incorporated in our system (as in Figure 11). A higher ξ, shifts the second "dip" in Figure 10 upwards, which allows use of a lower-keV beam.

R. Autrata: In the section "Solid scintillating BSE detectors", you report that 40% of the initial light passes through the light guide toward the PMT. It is known that the light passage depends on the guide material (index of refraction and absorption spectrum), wavelength of the passing light, shape and surface treatment of the light guide. What material was used for your light guide, and how was it shaped? What do you deduce the 60% light absorption in the light guide from? The light loss is extraordinarily high.

Author: It appears that, between us, we use some expressions corresponding to different objects: in your works, I think, you distinguish a "light guide" from a "light pipe", where the first leads to the second. In the present paper, I lump both of these parts under the term "light pipe". The initial part of my light pipe is what you term as light guide, but I have not seen the purpose for distinguishing these two parts (at least not in the present paper). This may explain why you find a 60% light loss in the "light guide" as extraordinarily high. In my example, I consider that 40% of the total photons produced at the BSE/photon conversion stage reach the photocathode. The difference is lost on the way (any way). The same figure of 40% transmitted light was quoted by Wells, and I use it for the typical SEM case. This was done to demonstrate that there is ample scope for improving the light pipes (or detectors), as I state. I have reported special shapes of light pipes (my term) with light transmission around 50% (Danilatos, 1985). I would have no hesitation to accept better transmission rates whenever these are found and shown to be possible, and this is the spirit of the present report.

R. Autrata: You say that "by the appropriate specimen positioning, PLA1 size and bias we can achieve a very good separation of the BSE from the SE signal." Can you give parameters of V1 and V4 voltages (Figure 11) and other conditions under which the separation of the SE from the BSE signal occurs? Can you really obtain the true SE image? Is it not a mixture?

Author: One example is to use a few tens of volts for V1 and a few hundreds of volts for V4 (both positive)

with a few hundreds of Pa pressure. The SE that get though PLA1 receive a preferential amplification over the BSE that also get though the aperture. I am referring to using the GDD alone for imaging in this case. It is true that the two signals are in mixture, but if, say, 90% of the intensity is due to SE and 10% of it to BSE, then we can safely classify the image as a SE one. We have obtained results of SE imaging above the PLA1, under these conditions, not yet reported. However, there are other electrode configurations by which we have reported good separation of the two types of imaging elsewhere (Danilatos, 1990c). In the present report, we are proposing to integrate the GDD with solid scintillating detectors to achieve a much more flexible system, with more powerful (deliberate) signal mixing, separation and processing, in general.

R. Autrata: Under the heading "Standardization of BSE Detector Efficiencies", you say that "ESEM has now ushered the possibility of using solid scintillating BSE detectors with a low-voltage beam without the need to accelerate the BSE in the keV range, as is usually done with low-voltage in vacuum." However, the need to accelerate BSE at low-voltage operation does not result from the BSE energy loss which occurs during the passage of BSE through the conductive coating of the scintillator. It is possible to prepare conductive layers on YAG with energy absorption less than 20% for the 1 keV electron beam energy. A more serious problem is the dependence of the light signal of the scintillator on the energy of incident electrons. The light signal of the scintillator produced by the BSE impact is very low at the 1 keV electron beam energy. The difference in the number of photons incident on the first dynode of PMT is one order for 10 keV beam energies. The resulting low SNR is the reason for accelerating the BSE toward the scintillator. Do you have some experimental experience in using ESEM low-voltage operation and an uncoated scintillator for BSE detection?
Author: I agree that the difficulty is caused by the fact that at low-voltage operation we start with only a relatively small amount of photons at the BSE/photon conversion stage. This difficulty should not be interpreted as the root cause for the inability to use unbiased detectors in conventional SEM at 1 keV. The presence of a conductive layer, conventionally an aluminum layer, has **significantly** contributed to signal energy losses at this early conversion stage and, hence, in the prevention of the use of the very **low-keV range** without accelerating the BSE. An aluminum coating will absorb all the BSE with 1 keV beam. The use of light pipes without optimum transmission and coupling with the PMT are additional factors, and all together have prevented the conventional SEM from operating in such a mode. The special conductive layers that you are referring to are not yet widely known or practiced, and they may help for some special detection requirements in our universal ESEM. However, as you say, even these layers absorb 20% of energy, and, hence, they must come second to using a minimum gas layer over the specimen, instead.

For high keV, the noise bottleneck is at the number of BSE incident on the uncoated detector. For low keV, the noise bottleneck is at the number of photoelectrons incident on the first dynode of the PMT. In Figure 10, I have assigned the second minimum ("dip") of the signal to the photocathode itself, as I have tacitly assumed that all the photoelectrons are collected by the first dynode. I have assumed that the PMT manufacturer has provided the best possible design of photocathode/dynode configuration. Assuming an optimum PMT, Figure 10 describes which variables are left for us to manipulate so that we can design an over all optimum detection system. For low-keV work, we both agree that the noise bottleneck is at the photocathode/first-dynode stage, and the most critical factor becomes the choice of photocathode material and its condition. This relies entirely on the PMT manufacturer. Given the best choice of PMT, we are then faced with optimizing the previous stages in the detection chain as outlined in the present paper. We have preliminary results of operation at low voltage with uncoated scintillator for BSE detection and a proper report will be made in due course.

D.E. Newbury: Since, as the author himself notes, water vapor is the preferred gaseous medium in ESEM, what are the expected general trends for the influence of such a polar molecule on the various gas thickness calculations as compared to nitrogen or argon?
Author: The theoretical scattering cross-section for the water molecule is less than that of nitrogen, and preliminary experimental values are even below the theoretical value. This has been confirmed by practice during imaging, where better results are achieved with water vapor than with nitrogen. A survey of scattering cross-sections for various gases has been presented previously (Danilatos, 1988). Good experimental measurements on many gases that can be of use in ESEM are still lacking, and we would welcome results from other laboratories that could dedicate some work in this area.

D.E. Newbury: I find it difficult to believe that you can place much hope that the efficiency of the GDD can be significantly improved based upon the experience with nuclear devices: (**1**) Nuclear particle detection generally involves particle energies in the MeV range rather than the low-keV range with which we deal in the SEM. (**2**) In nuclear particle detection there is no issue

of keeping a beam sharply focussed, as there is in the ESEM.

Author: (1) In nuclear physics, there is also an interest to detect electrons with insufficient energy to produce immediate ionization (i.e., like our SE). See, for example, "Single electron detection in proportional gas counters" [Genz H (1973) Nuclear Instruments and Methods **112**, 83-90] and "Electron multiplication process in proportional counters" [Raymond G, Bennett EF (1966) Physical Review **147**, 201-213]. (2) I agree that in nuclear particle detection there is no issue of keeping a beam sharply focussed. In the beginning, it was not obvious that those methods would work in our field. A lot of experimental and theoretical work had to be done. This is where our contribution lies. One of the novelties in ESEM is that we have successfully transferred nuclear methods to electron microscopy. It works, and it works well, indeed! For a thorough and detailed investigation please refer to Danilatos (1990a).

D.E. Newbury: No mention is made of the **critical issue** of the possibility, or lack thereof, of X-ray microanalysis in the ESEM. In any discussion of the relative intensities of the beam and skirt, the utility of such a beam for X-ray microanalysis should be considered. It seems clear that when the ESEM is operated at such high pressures that 67% of the electrons are located in the skirt, such a beam is useless for any realistic microanalysis applications. It would be interesting to consider what could be achieved in X-ray microanalysis with the ESEM operating at the other end of the scale, that is, a pressure such that water can just be retained. What is the beam/skirt ratio, and how degraded are X-ray spectra obtained from small objects such as 5 micrometer diameter inclusions in a matrix? The author may regard this topic as outside his range of "critical issues", but considering the claims made for the ESEM relative to the conventional SEM, the X-ray microanalysis shortcomings of the ESEM should be ventilated.

Author: I am fully aware of the importance of X-ray microanalysis and associated complexities in ESEM. Because this topic is quite extensive and relatively little work has been done in ESEM up to the present, I had opted to leave it out of this paper. There are many more critical issues that have not been dealt with in the present work. Only **some** issues have been considered. You are correct, though, that I should have mentioned it. It is only that I wanted to reduce the amount of speculation and restrict the contents only to the more obvious cases. I can only make a few suggestions here: one or more of the detectors in Figure 11 can be replaced with an X-ray detector. With a high-pressure environment, one way to remedy the interference of the skirt is to make the skirt very small. This can be achieved by placing the specimen so close to the PLA1 that the skirt radius is of the same order of magnitude as the beam-specimen interaction volume. This approach is facilitated by use of high keV in conjunction with a small PLA1, whereby the low magnification is traded off for high magnification. This approach has not been practiced yet, because, for best results, it requires the positioning of X-ray detectors above the PLA1, which implies the integration of these detectors with the lens system. An alternative solution to the question of electron skirt has been to subtract a calibrated percentage of a "raster" spectrum from a spot spectrum [Bolon RB (1991) X-ray microanalysis in the ESEM. In: Microbeam Analysis--1991. Howitt DG (ed.). San Francisco Press, 199-200]. The idea is to somehow calibrate out the effects of skirt.

For a fully wet specimen, the effects of skirt remain severe. However, for insulating specimens, we only need a very small amount of gas to dissipate charging, and this is an area where X-ray microanalysis can be practiced in the usual way in ESEM. It should be realized that ESEM is still at its infancy of development and is crying out for contributions by experts in various fields as those working in X-ray microanalysis.

I share your concern about the loss of spatial resolution with X-ray microanalysis at high pressure and long working distance range. At present, my best answer to this is that I believe that a solution and a method for this problem will be found in the near future.

D.E. Newbury: The comment "Low-voltage ESEM clearly offers all the advantages without any of the limitations of SEM" is clearly wrong. Low voltage SEM is limited in its resolution by the decreased brightness of the source. For FE-SEM (field emission SEM), reasonably high resolution can still be obtained because of the inherent brightness of the source, but for LaB_6 or conventional tungsten sources, the brightness limitation is much more significant. If the inevitable ESEM loss of beam electrons due to gas scattering is considered, the resolution will be even poorer. It therefore seems that ESEM has a significant disadvantage relative to the SEM when resolving power is considered. Finally, low-voltage X-ray microanalysis is indeed possible in the conventional SEM, but microanalysis is impossible in a microscope where 50% or more of the beam electrons are found in the wide skirt of the beam.

Author: ESEM, like SEM, can be used with all three types of guns, not only with tungsten and LaB_6 as the ElectroScan ESEM currently operates. Nikon Corporation has recently announced a FE ESEM, which has been adapted as a Critical Dimension Measuring SEM to serve in the electronics industry. Furthermore, ESEM,

like a SEM, can be used with all ordinary modes of detection. On the X-ray mode, I commented previously.

The question of resolving power in ESEM requires two steps of approach. The first step is to establish whether the **useful spot** spreads or not. It has been found that the unscattered electron beam fraction is clearly separated out from the skirt which is orders of magnitude larger. This is very significant, because, otherwise, the electron skirt would produce a first order, i.e., a **gross** deterioration of the spot diameter (i.e., if it were distributed in the immediate neighborhood of the original spot (see extensive study by Danilatos, 1988)). **In this connection**, we state that the resolving power is the same as in vacuum, and this has been demonstrated in practice. The second step is to consider the intensity of a fixed diameter spot. This step has been considered quantitatively with a formulation of SNR relationships (Danilatos, 1988). It has been acknowledged that, with a loss of beam electrons, we lose some of the ultimate possible resolution but this loss is not gross or catastrophic under the normal operating conditions of ESEM. Your question is ultimately reduced to quantifying the "losses" and "gains" in the ESEM. The parameter of gas pressure may be considered as the independent variable which determines the limits (or range) of operation of all other variables (or parameters). Some of those other variables are the accelerating voltage, beam current, specimen positioning (distance and tilt), temperature and detection efficiency. They, in turn, determine a host of other variables such as beam spot, contrast and resolution, specimen stability, etc. In this work, it has been attempted to show that ESEM can be made to operate in the complete pressure range from high pressure to high vacuum. Formally, then, we can state that

$$\textit{Universal ESEM} \xrightarrow[p \longrightarrow 0]{} \textit{SEM}.$$

The art of establishing the interrelationships and ultimate physical, limits of operating parameters, as we vary the pressure of gas in the specimen chamber of the microscope, constitutes the science of ESEM. It is a "give-and-take" situation as we vary the pressure, but, more precisely, practice has shown that it is much more of a "take" and much less of a "give" situation. Under this light, we can firmly state that SEM is a partial case of ESEM. The ESEM can be reduced to a SEM. Therefore, to make the previous statement unambiguous, we have introduced the modifier universal so that we can state: the universal ESEM offers all the advantages without any of the limitations of SEM (i.e., limitations associated with the vacuum condition).